Journal of Medicinal Chemistry

Article

pubs.acs.org/jmc

Maximizing Diversity from a Kinase Screen: Identification of Novel and Selective pan-Trk Inhibitors for Chronic Pain

Shawn J. Stachel,* John M. Sanders, Darrell A. Henze, Mike T. Rudd, Hua-Poo Su, Yiwei Li, Kausik K. Nanda, Melissa S. Egbertson, Peter J. Manley, Kristen L. G. Jones, Edward J. Brnardic, Ahren Green, Jay A. Grobler, Barbara Hanney, Michael Leitl, Ming-Tain Lai, Vandna Munshi, Dennis Murphy, Keith Rickert, Daniel Riley, Alicja Krasowska-Zoladek, Christopher Daley, Paul Zuck, Stephanie A. Kane, and Mark T. Bilodeau

Departments of Medicinal Chemistry, Biological Chemistry, Pain & Migraine, Molecular Systems, and Structural Biology, Merck Research Laboratories, P.O. Box 4, West Point, Pennsylvania 19486, United States

Supporting Information

ABSTRACT: We have identified several series of small molecule inhibitors of TrkA with unique binding modes. The starting leads were chosen to maximize the structural and binding mode diversity derived from a high throughput screen of our internal compound collection. These leads were optimized for potency and selectivity employing a structure based drug design approach adhering to the principles of ligand efficiency to maximize binding affinity without overly relying on lipophilic interactions. This endeavor resulted in the identification of several small molecule pan-Trk inhibitor series that exhibit high selectivity for TrkA/B/C versus a diverse panel of kinases. We have also demonstrated efficacy in both inflammatory and neuropathic pain models upon oral dosing. Herein we describe the identification process, hit-to-lead progression, and binding profiles of these selective pan-Trk kinase inhibitors.

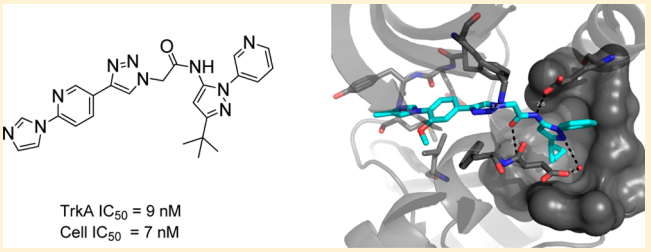

INTRODUCTION

Kinases are a class of enzymes whose primary function is to transfer the terminal phosphate group of ATP to an acceptor. For a major subclass of kinases the acceptor is another protein. This phospho-transfer event, termed phosphorylation, induces a conformational change in the receiving protein, resulting in a change in functional activity. This change in function is manifested in a diverse array of signal transduction processes within a cell and influences a wide array of cellular processes. Kinases are grouped into two main classes by cellular location, receptor and intracellular kinases. Receptor kinases propagate transmembrane signaling events, whereas intracellular kinases initiate signal transduction to the nucleus. In fact, kinases are so integral to biological processes that greater than 500 kinases have been identified, representing close to 2% of the human genome.[1] In totality, it has been stated that approximately 30% of all human proteins may be modified by kinase activity. Given that kinase signaling plays a ubiquitous role in physiological processes and the fact that ATP is the conserved ligand for all kinases, selectivity becomes paramount for the development of a safe and effective pharmaceutical agent. As such, achieving high selectivity against other kinases is a prerequisite for the development of clinical kinase inhibitor candidates.

Tropomysin receptor kinases (Trks) are cell surface receptor kinases that are highly expressed in neurons and play an important role in cell signaling.[2] There are three known members of the Trk family: TrkA, TrkB, and TrkC. All three of the Trks' polypeptides are composed of three distinct topological domains: an extracellular domain, a transmembrane domain, and a cytoplasmic kinase domain. Activation of the receptor occurs when a complementary neurotrophic partner binds with the extracellular domain of these kinases. Binding results in dimerization and subsequent autophosphorylation, thereby initiating the intracellular signaling pathway. Each of the Trks binds to a specific neurotrophic factor, and the complementary neurotrophin for each of the Trks is NGF for TrkA, BDNF for TrkB, and NT-3 for TrkC. We were particularly interested in the NGF/TrkA pathway because it plays a central role in the biology of chronic pain.[3,4] Activation of the receptor tyrosine kinase TrkA by NGF triggers intracellular signaling cascades and protein expression that increases the sensitivity of nociceptors leading to chronic sensitization and pain. Inhibition of the NGF/TrkA pathway has been validated clinically using NGF-neutralizing monoclonal antibodies that are currently in phase II−III trials for osteoarthritis pain.[5] We were interested in identifying small-molecule inhibitors of TrkA as an alternative intervention modality for the treatment of chronic pain.

Received: May 1, 2014

   dx.doi.org/10.1021/jm5006429 | J. Med. Chem. XXXX, XXX, XXX−XXX

HTS EFFORT

As part of our effort to identify selective inhibitors of TrkA, we conducted an HTS campaign with the intent of identifying nontraditional chemotypes as a starting point for discovery efforts to maximize the potential for increased selectivity versus the known kinome. Approximately 30K compounds were identified in the initial HTS campaign that displayed at least 30% activity toward TrkA, the kinase of interest (median Z' is 0.81; hit rate at 3σ is 0.5%). To narrow the number of active hits derived from the high throughput screen, we employed a number of filters. We removed hits that displayed promiscuous activity, defined as being active in more than five HTS campaigns or more than two kinase HTS campaigns. In addition, compounds were also counterscreened against the receptor tyrosine kinase insulin-like growth factor receptor 1 (IGFR1) serving as a general kinase for initial selectivity assessments. Lastly, activity against TrkA was measured using both low (0.1 mM) and high (2 mM) ATP concentrations to inform on potential ATP competitive binders. We succeeded in identifying a number of potentially interesting candidates to investigate further. Four particularly noteworthy compounds that showed modest activity against TrkA and at least a 50-fold selectivity window versus IGFR1, emerged from this effort, are exemplified in Figure 1. Compound **1** originated from a general

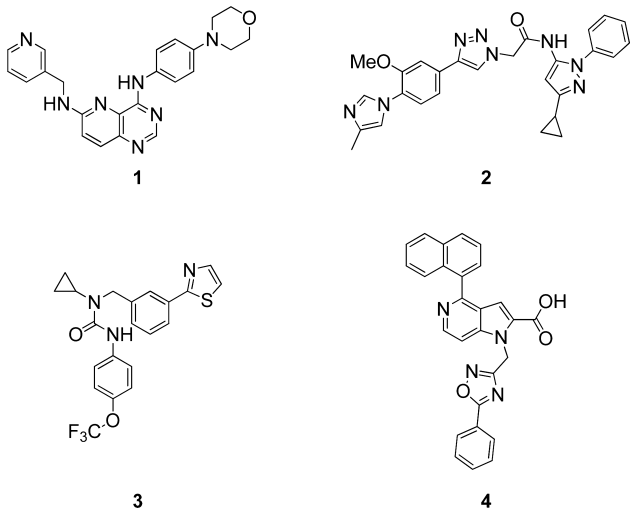

Figure 1. HTS leads.

kinase library but was chosen for further investigation because, while it contained a known chemotype used in orthosteric kinase inhibitors, it exhibited high selectivity versus IGFR1 (IC_{50} > 50 μM) and as such was followed-up on as a starting reference point for our crystallization efforts. In contrast, compounds **2**–**4** were all derived from non-kinase programs and, upon initial ocular inspection, did not resemble chemotypes typical of ATP-competitive binders. We chose to investigate these four compound classes in more detail as hit classes of interest with the goal of elucidating their binding profiles and further optimizing both their intrinsic potency toward TrkA and their physical properties.

Class I: Pyridopyrimidine Series. The pyridopyrimidine series, exemplified by the high-throughput screening hit **1**, displayed modest potency toward TrkA, $IC_{50} \approx 1$ μM, but as mentioned, **1** displayed favorable selectivity against IGFR1. When assayed against a broader 92-member kinase counterscreening panel, compound **1** exhibited only two hits of greater than 20% activity at 1 μM and <10% activity against the remaining kinases tested.[6] Initial efforts focused on obtaining increased potency toward TrkA to better gauge its relative selectivity toward the greater kinome. In parallel with our screening efforts, we also pursued methods to obtain X-ray crystallographic data to support follow-up SAR development using a rational structural design approach. Toward this end, we succeeded in obtaining protein crystals of the TrkA kinase domain that were suitable for soaking with inhibitors to obtain structural data in a relatively high-throughput manner.[7] The crystallographic structure of **1** was obtained and was found to bind in the ATP-binding site as seen in Figure 2.[8] Figure 3

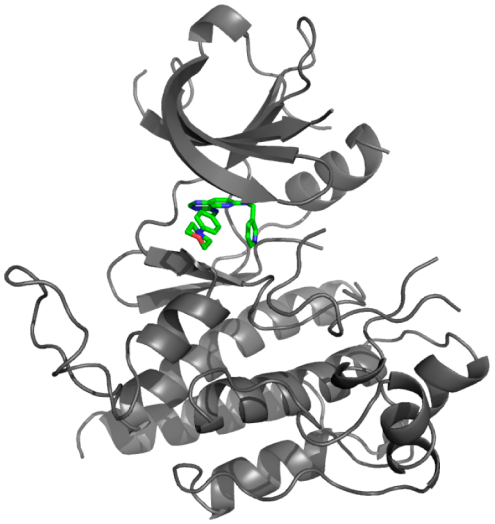

Figure 2. Crystal structure of **1** with TrkA. The compound binds in a DFG-in conformation.

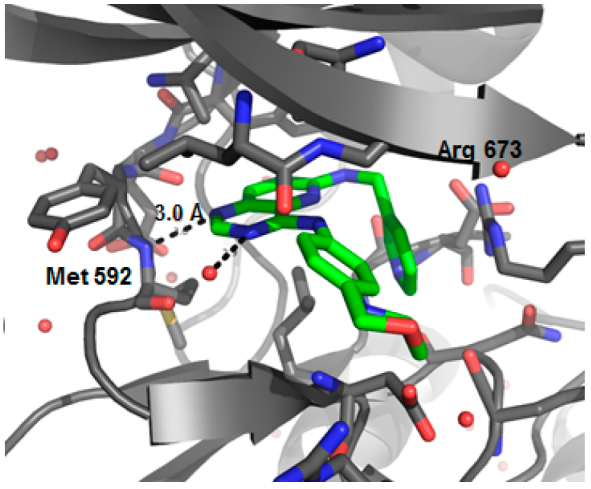

Figure 3. Hydrogen bonding interactions of **1** within the active site of TrkA.

depicts a magnified view of the ATP-site highlighting the binding interactions of **1** in the active site. The pyridopyrimidine was found to bind primarily within the hinge region of the enzyme and would be described as a type I, or DFG-in, inhibitor (vide infra).[9] The main hydrogen bonding interactions between the enzyme and inhibitor **1** occurs through a direct hydrogen bond between the N1 nitrogen of the pyridopyrimidine and the backbone NH of Met 592. The

dx.doi.org/10.1021/jm5006429 | J. Med. Chem. XXXX, XXX, XXX–XXX

benzylic pyridine portion of the molecule is tucked in the front pocket and forms a face-to-face π-stacking interaction with the guanidine group of the activation loop residue, Arg 673. The morpholine extends from the binding pocket into the solvent, which is consistent with the observation that morpholine and piperazine groups are commonly preferred substituents in this region of the binding pocket.[10]

Having elucidated the binding orientation of **1** to TrkA in the active site, we were able to pursue a rational approach for ligand optimization (Scheme 1). To track the progress of our optimization efforts in each series and to ensure that we were balancing any improvements in potency with the physicochemical properties of the molecule, we relied on optimizing ligand efficiency metrics based on both molecular mass (LE) and lipophilicity (LLE). Our optimization efforts in the pyridopyrimidine series began with replacing the morpholine ligand in the solvent exposed region with an *N*-methylpiperazine group, which as previously mentioned is another generic preferred substituent in the hinge/solvent front region of kinase inhibitors. In addition, since the pyridyl nitrogen in the western portion of the molecule did not appear to be making a productive hydrogen-bonding interaction with the protein, we investigated alternative substituents in the region by screening of a variety of benzylic amines and identified meta-chlorobenzylamine as a superior replacement. These two key modifications resulted in compound **5** that displayed a 90-fold enhancement in intrinsic inhibitory activity toward TrkA (Scheme 1). In addition, while **1** displayed activity of greater than 10 μM in the TrkA cell-based assay,[11] the potency improvements realized in **5** now afforded activity in our cellular assay. More importantly, **5** retained a high degree of selectivity displaying only three hits of greater than 20% activity at 1 μM against the 92-member kinase panel with a majority still showing <10% activity against the kinases tested. However, while overall ligand binding efficiency increased with these modifications (compound **5** LE = 0.33 vs compound **1** LE = 0.27), comparison of the lipophilic ligand efficiencies, LLEs (compound **5** LLE = 1.38 vs compound **1** LLE = 2.19) revealed that much of the improved potency was derived from lipophilic interactions.

Upon further optimization, the benzylamine was replaced with a difluoropyrrolidine as part of a scaffold hopping exercise incorporating structural motifs found in other known kinase inhibitors.[12] Next, screening a variety of aniline replacements identified a benzylic imidazothiazole as a preferred substitution resulting in compound **6**.[13,14] The synthesis of compound **6** is described in Scheme 2. Compound **6** displayed impressive single digit nanomolar activity toward TrkA, IC_{50} = 1.5 nM, as well as greatly improved potency in our cell-based TrkA assay, IC_{50} = 13 nM. The increased potency realized with **6** was also commensurate with improvements in ligand efficiency with respect to both molecular mass (LE = 0.36) and lipophilicity (LLE = 3.16).

Compound **6** was a very interesting lead that exhibited a typical type I kinase inhibitor binding mode. However, in parallel with optimization of **1**, efforts also continued on some of the other hits identified in the screen that originated from non-kinase programs with the hopes of elucidating additional inhibitors with more novel binding characteristics.

Class II: Phenyltriazole Series. A second series of interest focused on the HTS lead exemplified by compound **2**. This compound was originally synthesized as part of a legacy neuroscience program and did not constitute a lead originating from a prior kinase program. While **2** displayed modest potency toward TrkA, IC_{50} = 662 nM, it displayed a very favorable selectivity profile registering only one hit greater than 20% at 1 μM in the panel of 92 diverse kinases with the majority showing <10% activity against the kinases tested. Since the structure bore little resemblance to traditional ATP-site binding motifs for kinase inhibitors, we conducted a more detailed investigation of this structural series. Gratifyingly, we were able to obtain crystallographic data of **2** binding with TrkA.[15] In contrast to the type I, or DFG-in, binding mode described above for **1**, compound **2** was found to bind to a very different conformational form of the enzyme, commonly referred to as a type II, or DFG-out, conformation.[16] The differences between

Scheme 1. Evolution of Pyridopyrimidine HTS Lead 1

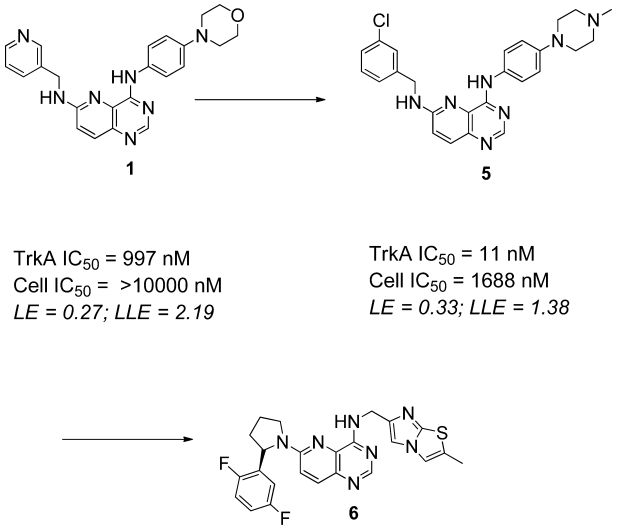

Scheme 2. Synthetic Route for Compound 6[a]

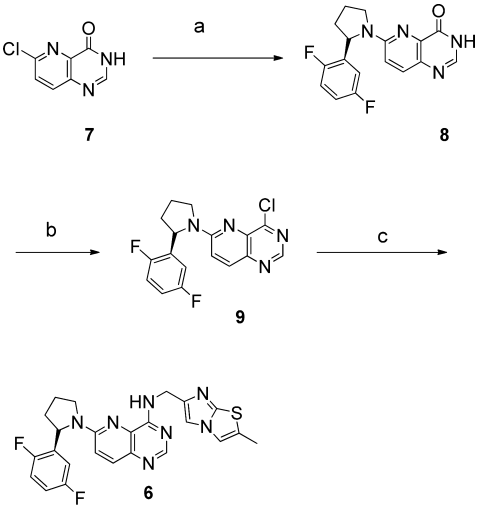

[a](a) (*S*)-2-(2,5-difluorophenyl)pyrrolidine, EtOH, 69%; (b) $POCl_3$, 70%; (c) 1-(1*H*-benzimidazol-2-yl)methanamine, EtOH, 58%.

dx.doi.org/10.1021/jm5006429 | J. Med. Chem. XXXX, XXX, XXX−XXX

type I and type II inhibitors go beyond the interactions of the inhibitor with the enzyme and involve substantial differences in the tertiary structure of the kinase itself. The primary function of a kinase is to transfer a phosphate group from ATP to another protein substrate in order to initiate a signaling cascade. For a number of kinases, this is regulated by a conformational change in a conserved triad of amino acids, composed of an Asp-Phe-Gly, or DFG sequence, at the start of the activation loop. To propagate the signaling cascade, the inactive kinase is first phosphorylated on its activation loop by an upstream kinase. In the case of the Trks this is accomplished through an autophosphorylation event brought about by dimerization of the enzyme upon binding to its corresponding neurotrophic factor. Once the activation loop is phosphorylated, it undergoes a conformational change that results in an opening of the active site. This conformation of the enzyme is termed the DFG-in conformation. This opening of the active site allows ATP to bind and subsequently transfer its terminal phosphate group. Conversely, in the inactive or nonphosphorylated state, the activation loop occupies the active site and prevents ATP from binding.[17] This closed conformation is termed the DFG-out conformation where the DFG segment is rotated out and toward the ATP binding site. The conserved DFG triad plays an integral part in inducing the requisite tertiary structure involved in kinase function. In the active form of the kinase the Asp (**D**FG) residue plays a critical role by coordinating with a magnesium ion that is also bound to the γ-phosphate of the ATP, thus serving to facilitate the phospho-transfer event. From a structural perspective, in the active form of the enzyme, the Phe of the D**F**G triad normally occupies a hydrophobic pocket located behind the gatekeeper residue allowing for proper positioning of the catalytic aspartate for the phospho-transfer event. However, in the inactive form the phenylalanine of the DFG triad is rotated out of its binding site behind the gatekeeper residue, thereby revealing a large hydrophobic pocket commonly referred to as the selectivity pocket. The fact that TrkA is able to adopt a DFG-out conformation is particularly unusual, since a small gatekeeper, typically valine or threonine, is often required to allow for this conformational transition, whereas in TrkA the gatekeeper residue is a large phenylalanine. Scientists at GNF have also reported a DFG-out binding conformation for their TrkA inhibitor series in a recent publication.[18] In fact, much of the recent efforts in the development of kinase inhibitors have focused on exploiting DFG-out binders, since they have been thought to hold potential advantages over active site orthosteric inhibitors. Since all kinases bind ATP as their orthosteric ligand, targeting the selectivity pocket has been viewed as a strategy to improve selectivity against the broader kinome. Several important new therapeutic agents have already been approved that selectively bind to the DFG-out kinase conformation, with the tyrosine kinase inhibitor imatinib being one of the most notable examples.[19] However, while the majority of human kinases contain the DFG-sequence as the start of the activation loop, only a relative few have been observed in both the DFG-in and DFG-out conformations.

As mentioned, compound **2** was found to bind to the DFG-out conformation of TrkA (Figure 5). Figure 4 depicts some of the key binding elements observed in the structure. First, the imidazole was observed to make one hydrogen bond to the hinge backbone NH of Met 592. The central triazole ring makes hydrophobic interactions with the gatekeeper phenylalanine residue, thus serving as a hydrophobic clamp for the

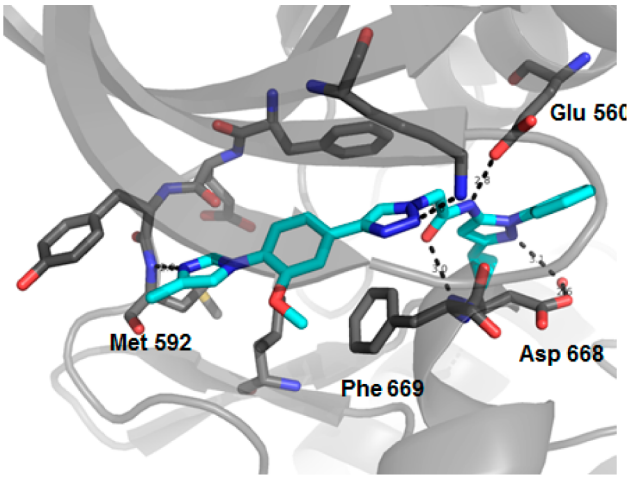

Figure 4. Hinge-binding interactions of **2**.

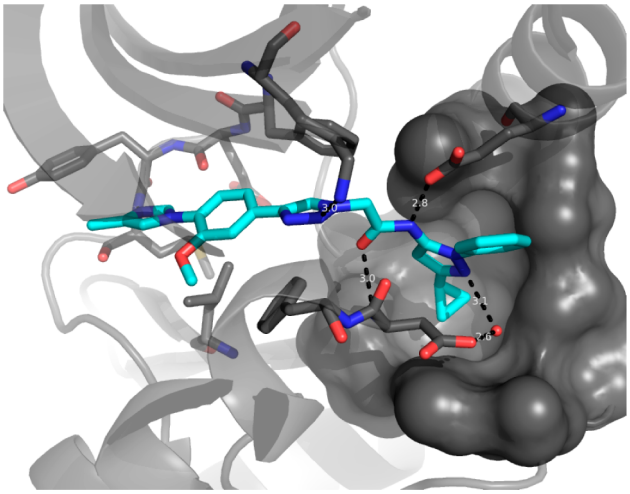

Figure 5. DFG-out binding of **2**.

inhibitor in the active site. The amide carbonyl forms a hydrogen bond with the NH of the catalytic Asp (668) residue and the amide NH hydrogen bonds to the carboxylate of Glu 560. The *N*-phenylpyrazole occupies the hydrophobic selectivity pocket normally occupied by Phe 669 in the active, DFG-in, kinase conformation, with the pyrazole nitrogen making an interesting water-mediated hydrogen bond to the carboxylate of the catalytic Asp 668.

SAR Optimization of 2. Having secured a crystal structure of **2** in the TrkA active site, we were able to leverage the structural information gleaned from our analysis of the binding mode to rapidly progress the series (Scheme 3). First, from the structure it was evident that the methoxy group on the western aryl ring of **2** was oriented toward the solvent front and was not participating in any meaningful interaction with the enzyme. As such, removal of the methoxy group (**10**) resulted in an improvement in both enzymatic and cellular potency, perhaps due to the conformational effect of the methoxy group that twists the imidazole/phenyl dihedral angle from coplanarity. Removal of methoxy allows the imidazole to attain coplanarity with the aryl ring, the proposed bioactive conformation, affording a 10-fold increase in potency. This modification also resulted in increased metrics for ligand efficiency with the LE increasing from 0.23 to 0.28 and LLE increasing from 2.08 to 3.16, signaling that the increase in potency was not being driven

dx.doi.org/10.1021/jm5006429 | J. Med. Chem. XXXX, XXX, XXX−XXX

Scheme 3. Evolution of Triazole HTS Lead 2

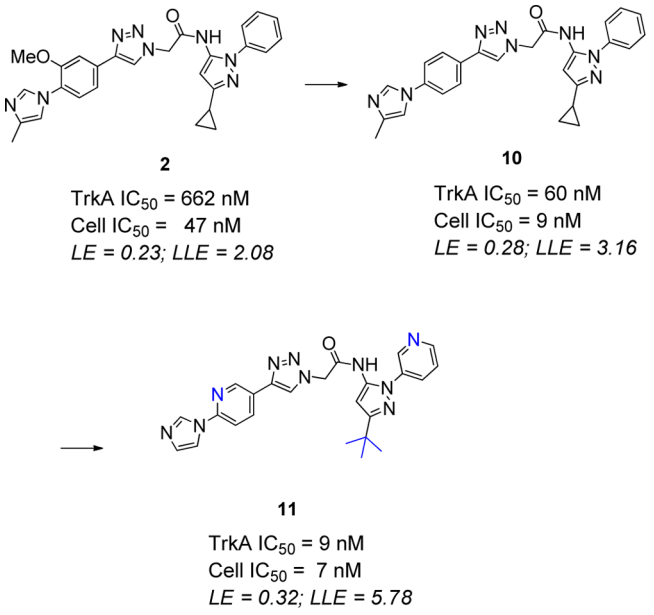

Scheme 4. Synthetic Route for Compound 11[a]

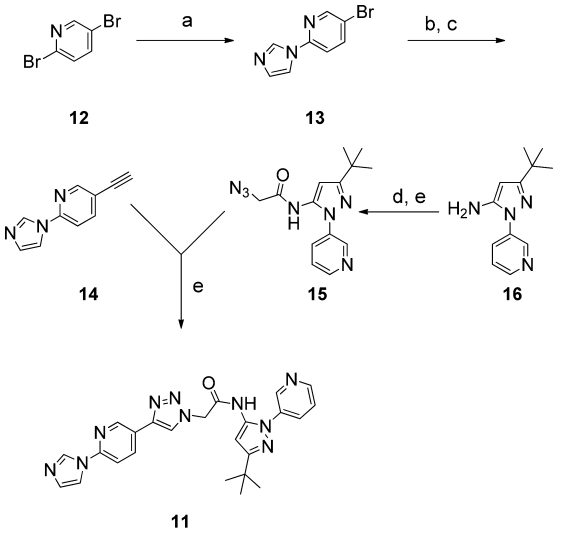

[a](a) Imidazole, L-proline, CuI, K_2CO_3, DMSO, 61%; (b) TMS–acetylene, $PdCl_2(PPh_3)_2$, CuI, Et_3N, DMF, 78%; (c) KF, MeOH, 100%; (d) 2-chloroacetyl chloride, Et_3N, CH_2Cl_2, 72%; (e) NaN_3, EtOH, 92%; (f) Cu powder, CH_2Cl_2–*t*-BuOH, H_2O, aq $CuSO_4$, 72%.

solely by lipophilicity changes. As mentioned in the above discussion, it was evident that **2** formed only one direct hydrogen bond with the hinge backbone. For our next modification we sought to increase the number of hinge binding interactions through the introduction of a nitrogen into the aryl ring in the form of an aminopyridine. However, instead of a direct interaction with the backbone, the X-ray cocrystallographic structure revealed that the nitrogen lone pair interacted indirectly with the carbonyl of Glu 590 through an intermediary water molecule. Modifications were also made to the portion of the molecule occupying the hydrophobic selectivity pocket. As such, the cyclopropyl group was changed to a bulkier *tert*-butyl group in order to more optimally fill the hydrophobic void previously occupied by the DFG-phenylalanine in the DFG-out conformation. In addition to this change, the introduction of a nitrogen to the pendent *N*-phenyl group served to decrease the overall cLogD by 1 log unit while not imparting additional hydrogen bonding interactions with the enzyme. The impact of this modification is apparent in the LLE value, as it increased to 5.78 from 3.16 for compound **11** when compared to **10**, indicating more efficient binding with lower overall lipophilicity. Taken together, these modifications that afforded compound **11** (synthesis described in Scheme 4) resulted in an additional improvement in both enzymatic and functional activity providing an inhibitor with single digit nanomolar activity in both the enzymatic and cellular assays. The changes to the starting structure not only led to increased potency but were accomplished by maintaining and improving ligand efficiency in a per atom binding basis and also with respect to the overall lipophilic character. Compound **11** retained the exquisite selectivity against the kinase panel showing high selectivity with the improved potency registering only nine hits with >20% inhibition at 1 μM with a majority showing <10% activity against the kinases tested. Compound **11** possessed the requisite potency and physical properties to be assessed in vivo and was found to be efficacious in our pain models (vide infra). It should be noted that the superior cellular potency compared with the enzymatic activity of this, and other series, is most likely a result of the effect of conducting the enzymatic activity assay at elevated ATP levels to facilitate an increased dynamic range in the enzymatic assay but that are not necessarily reflective of the native levels of ATP present within the cells.

Class III: Urea Series. A third series of interest focused on the HTS lead exemplified by compound **3**.[20] This compound displayed remarkable selectivity against all other kinases in the general counterscreen with 0 hits of >20% activity at 1 μM. Compound **3** was originally synthesized as part of our general screening library. While compound **3** did not overtly resemble a typical ATP-competitive chemotype, we now recognized that TrkA was capable of binding both DFG-in and DFG-out type inhibitors. Since amide and urea-based kinase inhibitors have been well documented in the literature and are typically DFG-out binders, at first glance it seems plausible that this inhibitor could also be interacting through a similar binding paradigm.[21−24] However, all of the reported inhibitors of this class are diphenyl amides or ureas and are involved in hydrogen bond donor and acceptor roles with the unsubstituted nitrogens which are both involved in key hydrogen bonding interactions with the enzyme. The potential for an atypical binding paradigm for **3** was reinforced when we performed docking experiments to suggest potential binding conformations. Unfortunately we were unable to achieve such convincing poses with the substituted ureas analogues. In fact, the fully unsubstituted urea (**19**) was found to be completely inactive in the enzymatic assay with an IC_{50} of >100 μM. By analyzing structurally similar compounds contained within the collection, we quickly found that an isopropyl group offered a 30-fold potency enhancement over the cyclopropyl derivative (**17**) (Scheme 5). Compound **17** also retained excellent selectivity with only one hit of greater than 20% activity when assayed against the 92-member kinase counterscreen. Concurrent with the aforementioned similarity assessment, we succeeded in obtaining a crystal structure of compound **3** with the TrkA kinase domain (Figure 6).[25] The structural information turned out to be quite revealing: the inhibitor was indeed found to bind to the DFG-out conformation of the kinase, as other amide and urea kinase inhibitors were already known to do, but

dx.doi.org/10.1021/jm5006429 | J. Med. Chem. XXXX, XXX, XXX–XXX

Scheme 5. SAR Progression of HTS Lead 3

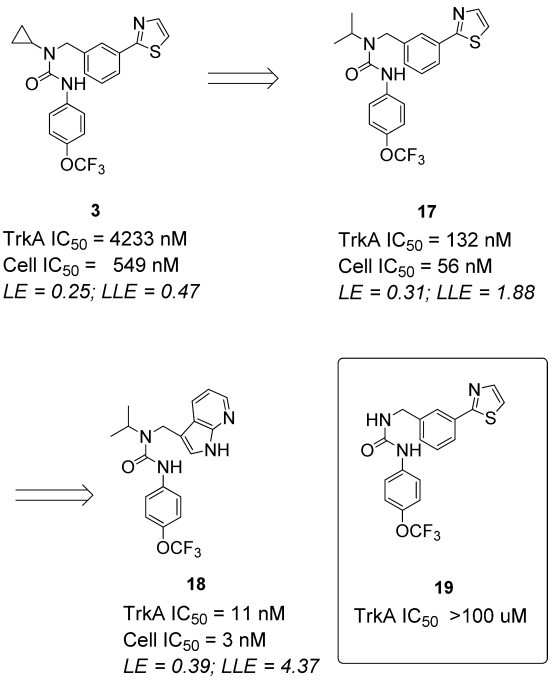

it did so without some of the more commonly observed characteristics. The thiazole occupied the ATP-binding site but was only found to form a weak hydrogen bond with Met 592. The benzylic aryl ring was involved in hydrophobic interactions with the gatekeeper residue, Phe 617. The para-trifluoromethoxyphenyl group was situated in the hydrophobic selectivity pocket normally occupied by Phe in the DFG-in conformation, as is typical in DFG-out inhibitors, and the amide carbonyl was shown to form a hydrogen bond with the catalytic aspartate (D668) as is typical with the literature precedence. The cyclopropyl group on the adjacent nitrogen was shown to occupy a hydrophobic cleft and was tucked neatly against Val 524. This is interesting, since inhibitors of most kinases are typically unsubstituted and involved in a hydrogen bond with the homologous residue of α-C helix Glu 560. Our interpretation of the SAR around this group is that a critical hydrophobic mass is required to fill the small pocket near Val 524, Ala 542, Lys 544, and Phe 589, perhaps to displace a water molecule that may otherwise unfavorably occupy this region.

Having solved the crystal structure and elucidated that the thiazole, while occupying the ATP binding site, was not making optimal interactions with the protein, we sought to replace it with an alternative heterocycle with a greater potential to make favorable hydrogen bonding interactions with the hinge. This was accomplished by replacement of the thiazole with an azaindole group and resulted in compound **18** (synthesis described in Scheme 6). Here the azaindole functions as a hydrogen-bond acceptor interacting with the NH of Met 592. Conversely, the indole NH serves as a hydrogen bond donor interacting with the carbonyl of Glu 590 in the backbone. Hence, optimization of the interaction with the hinge region and increasing the hydrophobic size of the heterocycle in the adenine site resulted in 10-fold improvement in both enzymatic and functional activity. It should also be noted that, similar to the two series previously described, optimization of the binding affinity for this series was also accomplished while maximizing the ligand binding and the lipophilic binding efficiencies.

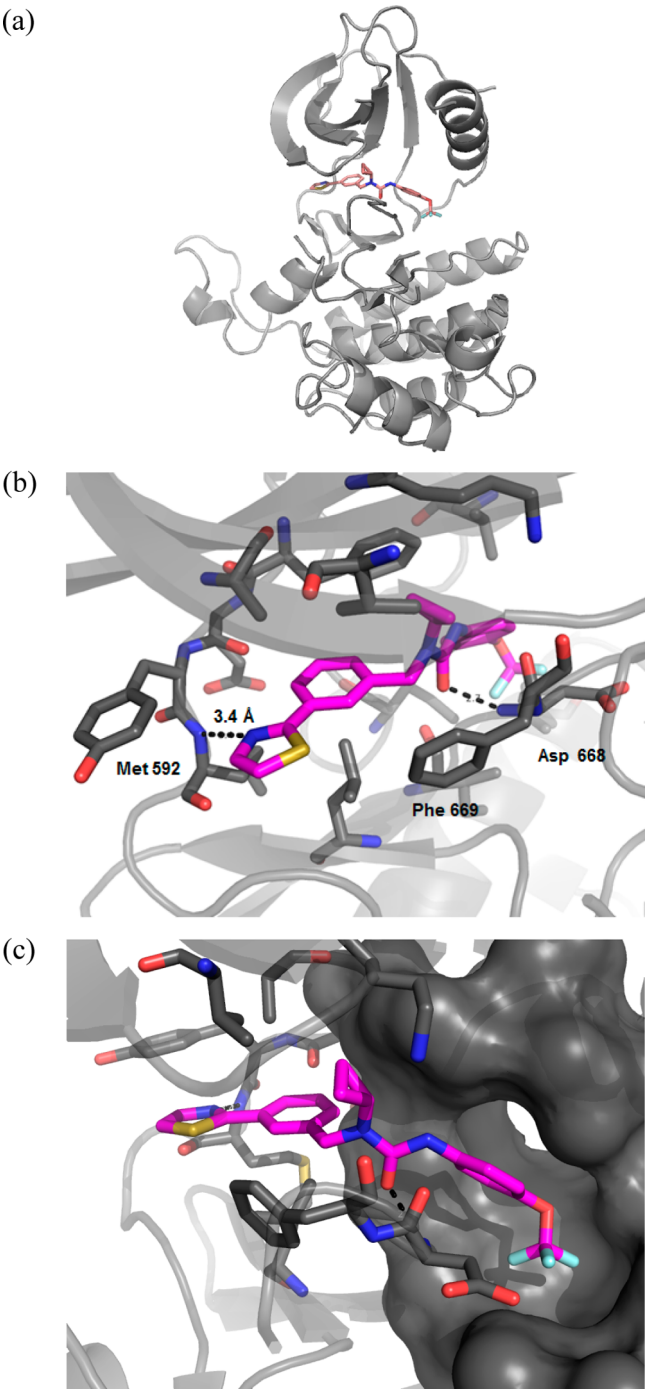

Figure 6. (a) Crystal structure of **3** bound with TrkA. (b) Hinge-binding interactions of **3**. (c) View of **3** bound in the selectivity pocket.

Class IV: Azaindole Series. The fourth and final series described here focused on the HTS lead exemplified by compound **4**. Pursuant to our strategy of investigating novel chemotypes, compound **4** was chosen for further investigation, since it displayed no activity against IGFR1 as part of the HTS counterscreening protocol. In addition, **4** showed no activity against any of the broader 92-membered kinase panel which was supported by our inability to dock this structural class into the TrkA active site, in either a DFG-in or DFG-out conformation, in a reasonable way. Intriguingly, while compound **4** was identified as a hit possessing moderate potency toward TrkA in the high throughput screen, i.e., IC_{50} =

dx.doi.org/10.1021/jm5006429 | J. Med. Chem. XXXX, XXX, XXX−XXX

Scheme 6. Synthetic Route for Compound 18[a]

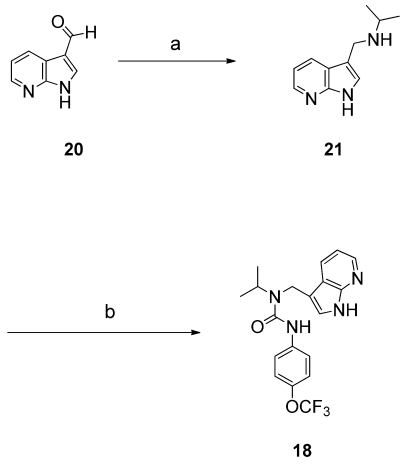

[a](a) Isopropylamine, $NaCNBH_3$, MeOH; (b) 1-isocyanato-4-(trifluoromethoxy)benzene, THF, 98% over two steps.

163 nM, when compound **4** was tested in our confirmation assay, it was found to display a severe disconnect between the screening and follow-up assays, exhibiting approximately a 100-fold difference in activity. The team was initially perplexed at the disparity between the two assays and sought to identify the cause for the difference in activity. In turned out that two slightly different assays were used for the HTS screen and subsequent confirmation assay, with the HTS screen utilizing a homogeneous time-dependent fluorescence (HTRF) assay, whereas the confirmation assay employed a caliper assay. More importantly, upon reinvestigation of the assay protocols, it was discovered that the TrkA protein used for the high throughput screen was nonphosphorylated protein whereas the protein that was used in the confirmation assay was provided as a phosphorylated TrkA protein. To investigate this phenomenon further, Thermofluor analysis was conducted using both forms of the protein, phosphorylated and nonphosphorylated. Compound **4** displayed a ΔT_m of 11 °C when assayed using the unphosphorylated protein. In contrast, no change in melting temperature was observed when the phosphorylated protein was utilized. These results provided support that compound **4** was exhibiting phosphorylation-state dependent binding. Phosphorylation state-dependent binding to kinases is an emerging avenue for inhibitor design. Since the DFG-out conformation represents the inactive, unphosphorylated protein, many compounds that exhibit this type of binding profile have shown differential binding activities between the active and inactive forms, but most DFG-out inhibitors are capable of binding both forms of the protein. However, there are several recent reports in the literature of inhibitor series that are active only versus the unphosphorylated form of the kinase of interest and have unmeasurable, or weak, inhibition of the phosphorylated form.[26,27] Having discerned the cause of discrepancy between the activity in the two assay formats, we subsequently assayed compound **4** in our caliper-based assay using nonphosphorylated TrkA protein. Under these conditions **4** displayed IC_{50} = 2300 nM. While the potency was improved under these conditions versus the 17 μM IC_{50} obtained using the phosphorylated enzyme, the IC_{50} was still ~10-fold higher than the original HTS HTRF IC_{50} of 0.16 μM. This shift can partially be explained by the difference in ATP concentrations between the assays. For the standard caliper-based assay we employed a higher ATP concentration (i.e., 10 mM) compared to the 2 mM ATP concentration used in the HTS screen allowing more effective binding competition and an upward shift in IC_{50} values. The shift to higher ATP concentrations for use in the follow-up assay was done to allow for more dynamic range in the assay for our optimization efforts. However, it should also be noted that it is difficult to determine if the original 17 μM IC_{50} observed when assayed using phosphorylated substrate was derived from residual levels of nonphosphorylated enzyme in the supplied protein and may not reflect an accurate IC_{50} against pure phosphorylated material. As such, the IC_{50} values for all subsequent compounds for this particular series were determined using nonphosphorylated enzyme to have measurable and consistent activity by which to conduct SAR analysis. Prior to determining the importance of the phosphorylation state for the enzymatic assay the series was progressed using the cell-based potencies, since the cellular system exists in a dynamic equilibrium between the active and inactive forms of the protein and provides a more physiological assessment of a compound's activity in the presence of endogenous ATP levels.

Binding of Azaindole Series. To elucidate the binding mode and obtain the structural insights necessary to design more potent inhibitors, we obtained the structure of compound **4** complexed with the TrkA kinase domain (Figure 7).[28] The structure clearly showed that **4** binds to the DFG-out conformation of TrkA. The structure revealed several unusual binding features for compound **4**. First, the inhibitor was found not to have a direct interaction with hinge backbone. Instead, the N5 nitrogen of the azaindole was shown to participate in a water-mediated hydrogen bond to two hinge residues, Asp 590 and Met 592. The naphthalene moiety was buried in the hydrophobic cleft at the front of the hinge flanked by the activation loop residue Met 670. This conformation was further stabilized through hydrophobic interactions with the DFG phenylalanine just behind the naphthyl ring inside the adenosine site. The isoxazole ring was situated under the gatekeeper phenylalanine residue, stabilized by hydrophobic van der Waals interactions and orienting the terminal phenyl ring into the selectivity pocket. One of the more unusual binding interactions was that of the indole carboxylic acid. Here the carboxylate was interacting with two backbone NHs in the activation loop, donated by Gly 671 and Met 670. A third hydrogen bonding interaction was also evident between the carboxylate and Lys 544 on the roof of the adenosine binding pocket. As stated previously, several of the inhibitors described previously were also found to bind to a DFG-out conformation but they did not show the phosphorylation-dependent binding that compound **4** exhibited. We believe that it is this unusual binding conformation between the indole carboxylate and the activation loop that leads to the phosphorylation-state dependent binding. This can be visualized in Figure 8, which depicts the interaction between Tyr 676 and Asp 595 in the crystallographic structure of TrkA bound to compound **4**. In this structure tyrosine 676 is involved in a hydrogen-bonding interaction with Asp 596. Since Tyr 676 is a known phosphorylation site on TrkA, it is apparent that phosphorylation of Tyr 676 would introduce a repulsive electrostatic interaction and disrupt this interaction with Asp 596, thereby forcing the activation loop away from the active site and thus stabilizing the active conformation. As such, the phosphorylated form of the enzyme is not able to adopt the tertiary conformation needed to bind compound **4** because of this

dx.doi.org/10.1021/jm5006429 | J. Med. Chem. XXXX, XXX, XXX–XXX

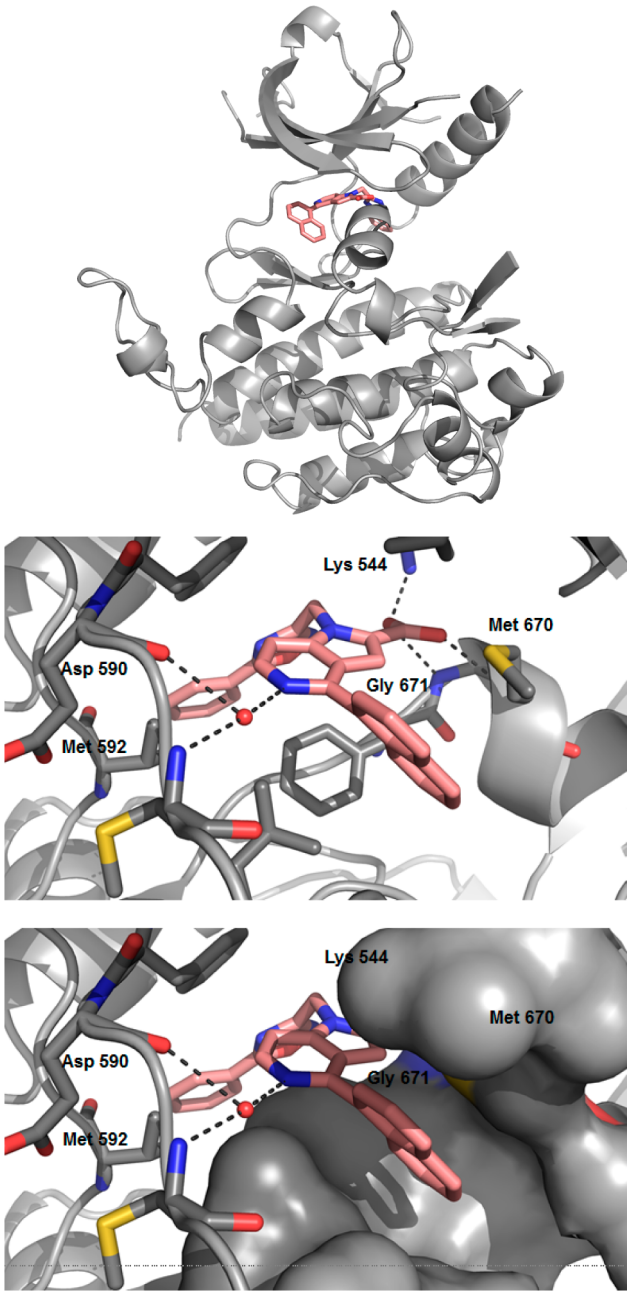

Figure 7. Binding pose of **4** in the TrkA active site.

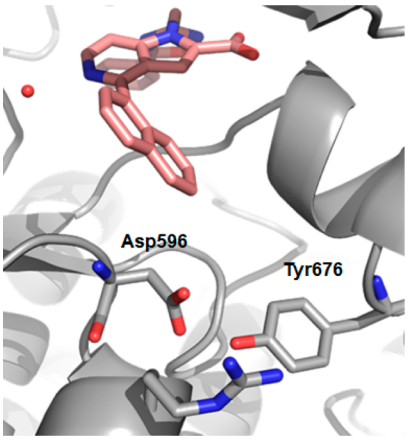

Figure 8. View of stabilizing interaction of inactive conformation.

Scheme 7. SAR Progression of HTS Lead 4

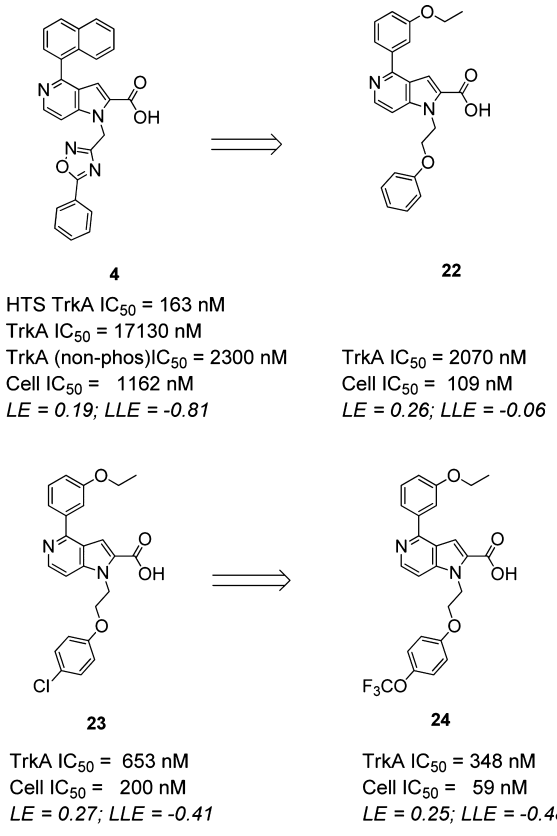

repulsive interaction. A second, similar interaction also exists between Asp 650 and Tyr 680 (not depicted), another known TrkA phosphorylation site.

SAR Optimization of 4. Having solved the structure and elucidated the key interactions of **4** with TrkA, we were now positioned to follow a rational design approach toward ligand optimization (Scheme 7).[29] First, the lipophilic naphthyl group that was found to bind in the hydrophobic cleft at the front of the hinge was replaced with a 3-ethoxyphenyl group. It was also discovered that the isoxazole could be replaced by a β-ethoxy linker (compound **22**), which maintained the linear orientation and trajectory for positioning of the arene ring into the selectivity pocket. These modifications resulted in approximately 10-fold improvements in both functional and intrinsic activities. It was also evident that the unsubstituted aryl ring did not optimally fill the selectivity pocket, presumably instead leaving an unfavorable water molecule at the bottom of the pocket. As such, a para-chloro group was added, providing compound **23**, which effectively displaced the water molecule and more efficiently occupied the hydrophobic cavity resulting in a further improvement in potency. This interaction was further optimized through the use of a para-trifluoromethoxy group (compound **24**) to more optimally fill the unoccupied space, as inspired by crystallographic overlays with compound **3**, resulting in an additional increase in potency (synthesis described in Scheme 9). While advances were realized toward increasing potency with concomitant increases in ligand efficiencies, it was apparent that the majority of the binding affinity was being derived from lipophilic interactions as represented in the low LLE values. In order to obtain more acceptable druglike physiochemical properties, we endeavored

dx.doi.org/10.1021/jm5006429 | J. Med. Chem. XXXX, XXX, XXX−XXX

to improve on this parameter by lowering the clogP of the series.

Introduction of Hinge Binding Interaction. In order to address the high lipophilicity of the series, we envisaged that further optimizing hydrogen bonding interactions with the hinge could provide increased affinity without adding to the lipophilicity of the molecule. We began by removing the very hydrophobic ethoxy arene that was involved in hydrophobic van der Waals interactions with the hydrophobic cleft to allow room for alternative substitution of the indole ring. While removal of this hydrophobic interaction resulted in a precipitous 35-fold loss in potency (compound **25**, Scheme 8), it should be noted that ligand binding efficiency stayed on par with compound **24** while the lipophilic contributions to affinity were improved, as is apparent in the increase in LLE to 0.61 for compound **25** compared with −0.48 for compound **24**. Since the indole N5 nitrogen lone pair was directed toward the backbone residue Met 592 with an intervening water molecule, we decided to introduce a nitrile group in an attempt to form a direct hydrogen bonding interaction with the backbone (compound **26**). Gratifyingly, this modification led to a 100-fold increase in both enzymatic and cellular potency. Finally, replacement of the nitrile with a pyrazole, a common hinge binding motif, led to compound **27** which has an IC_{50} value of 51 nM in the enzymatic TrkA assay and an IC_{50} of 29 nM in the TrkA cell-based assay. Thus, by removing a large contributor to lipophilic binding and focusing on optimizing the binding interactions with the hinge, we were able to significantly improve the LLE value while maintaining good overall per atom binding efficiency.

Selectivity against other kinases was somewhat difficult to assess for this series because of its unique phosphorylation-state dependent binding paradigm. As mentioned, **4** was inactive against IGFR1 in our original HTS screen. In addition when **4** was assayed against the full kinase panel, there was no activity noted against any of the 92 kinases. This was not entirely surprising, since all of the kinases used in the panel were presumed to be the active form of the protein; i.e., they were phosphorylated kinases. Since we already determined that **4** did not bind to the active, phosphorylated form of TrkA, it was conjectured that it would not bind to the activated forms of other kinases either. These results were also confirmed with compound **24**. In order to more fully assess the functional selectivity of this series, we submitted **4** and **24** to a panel of cell-based assays where the kinase should be in a dynamic equilibrium between the activated and unactivated states, but here again we were unable to detect any significant activity.

Binding Kinetics. Surface plasmon resonance (SPR) studies using Biacore were performed with several inhibitors to investigate differences in their binding kinetics. Rates for inhibitor association (k_{on}) and disassociation (k_{off}) with the enzyme were measured to reveal the underlying drivers of differences in the disassociation constant K_D (where $K_D = k_{on}/k_{off}$, Table 1). Compound **5**, which bound in a DFG-in conformation, displayed very fast on and off rates (yielding a "square wave" in the Biacore sensogram); fitting the plateau value gave a K_D in line with its intrinsic activity (K_D = 25 nM vs IC_{50} = 10 nM). In contrast, all of the inhibitor series that bound in the DFG-out conformation displayed significantly slower on and off rates with the enzyme. The triazole HTS lead **2** was shown to have a $k_{off} = 1.7 \times 10^{-3}$ s^{-1} ($t_{1/2}$ = 6.8 min); further optimization to **11** led to a dramatic reduction in the off rate, $k_{off} = 1.7 \times 10^{-4}$ s^{-1} ($t_{1/2}$ = 68 min). Similarly, in the urea

Scheme 8. Optimization of Hinge Binding Interaction with Azaindole Series

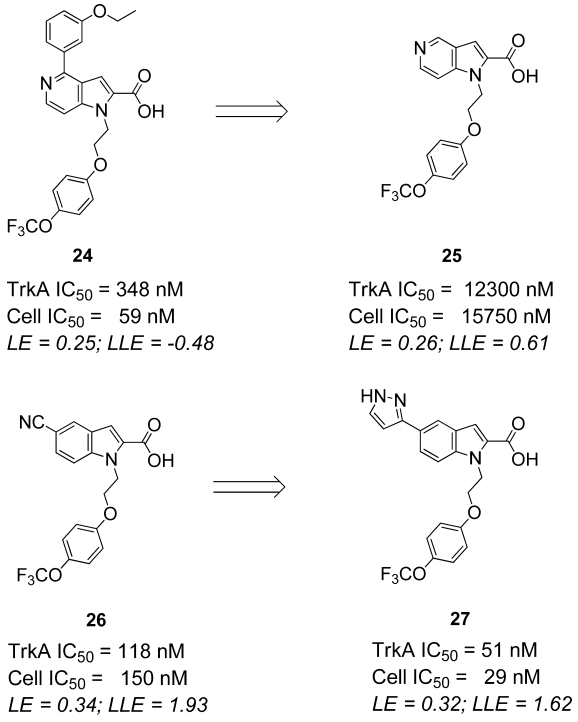

Scheme 9. Synthetic Route for Compound 24[a]

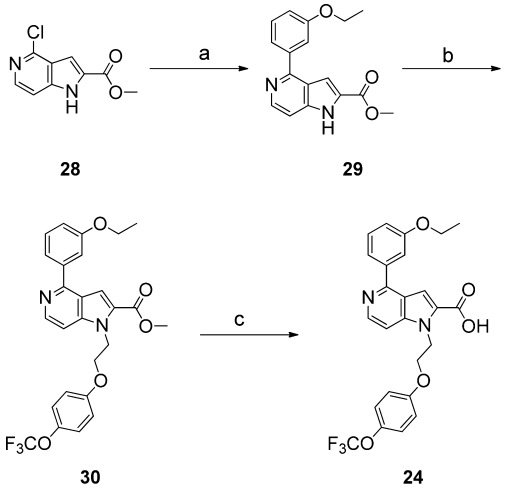

[a](a) 3-Ethoxyphenylboronic acid, $Pd(OAc)_2$, XPhos, KF, 1,4 dioxane 73%; (b) NaH, 2-bromophenyl ether, DMF, 1 N NaOH; (c) 2 N NaOH, 75% over two steps.

Table 1. Binding Affinity of Inhibitor Series

compd	k_{on} (M^{-1} s^{-1})	k_{off} (s^{-1})	K_D (nM)
5			63
2	62 000	1.7×10^{-3}	27
11	180 000	1.7×10^{-4}	0.94
3		1.5×10^{-2}	~400
17	30 000	1.9×10^{-3}	63
4	22 000	1.7×10^{-4}	7.9
23	26 000	9.0×10^{-5}	3.5

dx.doi.org/10.1021/jm5006429 | J. Med. Chem. XXXX, XXX, XXX−XXX

inhibitor series, the initial hit compound **3** displayed a relatively fast off rate of 1.5×10^{-2} s^{-1} ($t_{1/2}$ = 0.8 min) and $K_D \approx 400$ nM. Potency of the series was improved with compound **17**, and this tracked with a 10-fold improvement in disassociation constant, providing K_D = 63 nM that was driven by a 10-fold improvement in off rate, $k_{off} = 1.9 \times 10^{-3}$ s^{-1} ($t_{1/2}$ = 6 min). Finally, the azaindole series had the longest off rates of the four series investigated where the initial hit, **4**, displayed $k_{off} = 1.7 \times 10^{-4}$ s^{-1} ($t_{1/2}$ = 68 min). Interestingly, the dissociation constants for this series were much lower than the intrinsic potency compared to the other series. Here the disassociation constant for **4** had K_D = 7.9 nM versus IC_{50} = 2300 nM. Further optimization of this series resulted in compound **23** which displayed a 2-fold improvement in both K_D and residence time, K_D = 3.5 nM; $k_{off} = 9.0 \times 10^{-5}$ s^{-1}; $t_{1/2}$ = 128 min. Since the on rates remained relatively constant between the series, these results suggest that the increases in potency realized during lead optimization were largely driven by decreased off rates. This also suggests that DGF-out inhibitors should have significantly longer residence times on the receptor compared with DFG-in inhibitors. These data align with other type II binders that have also been reported to display lower disassociation rates and extended residence times.[30,31] This further highlights the advantages of targeting the DGF-out conformation in inhibitor design, since they not only have the potential to exhibit increased selectivity toward other kinases but may have the added advantage of slower off rates prolonging binding to the receptor.

In Vivo Activity. While efficacy for the TrkA pathway has already been established both clinically and preclinically, those studies were conducted using an anti-NGF antibody approach. We sought to validate the use of a small molecule TrkA inhibitor in preclinical in vivo pain models.[32,33] To support these studies, compound **11** was chosen because it exhibited excellent cellular potency and an extended residence time on the enzyme. As such, compound **11** was profiled in rats and displayed pharmacokinetic properties suitable for in vivo studies with a clearance of 16 mL min^{-1} kg^{-1}, a half-life of 2.6 h, an oral bioavailability of 30%, and a plasma protein binding of 99.5%. To fully explore the in vivo efficacy of a small molecule TrkA inhibitor, we investigated the effects of compound **11** in both an inflammatory and a neuropathic pain model. For the inflammatory pain studies, we employed the complete Freund's adjuvant-induced hind-paw (CFA) model. Compound **11** was dosed orally b.i.d. for 7 days after administration of the Freund's adjuvant, similar to previous studies using an anti-NGF antibody where reversal of allodynia was reported on day 3 through day 7 after treatment.[32] Figure 9 displays the percentage reversal of mechanical hypersensitivity at both the predose and 2 h postdose time points on day 7 of the study. As exemplified in Figure 9, compound **11** inhibited mechanical allodynia with naproxen-like efficacy at both the 30 and 100 mg/kg dose levels. Table 2 lists the plasma levels of compound **11** at the 2 h postdose time point. When corrected for plasma protein binding, significant effects are achieved at unbound drug concentration at or above the IC_{50} values obtained in the cell-based TrkA assay, with residual effects on mechanical allodynia remaining at the trough (predose, plasma levels were not obtained) prior to compound readministration. To investigate in vivo efficacy in a rat model for neuropathic pain, we employed the Chung spinal nerve ligation model where compound **11** demonstrated approximately a 50% reversal of mechanical hypersensitivity at the 100 mg/kg dose

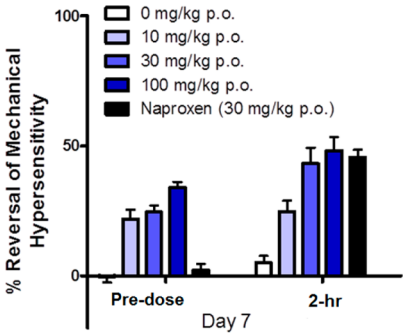

Figure 9. CFA-induced mechanical hypersensitivity assay (inflammatory pain) with compound **11**.

Table 2. Plasma Concentrations in CFA Study at 2 h

dose (mg/kg)	[plasma] (μM)	$C_{u,plasma}$ (nM)	fold IC_{50}
10	1–2	5–10	1–2 ×
30	4–9	20–45	4–9 ×
100	16–45	80–226	16–45 ×

(Figure 10), similar to the effect observed with the positive control, pregabalin. Here, similar plasma levels were obtained at

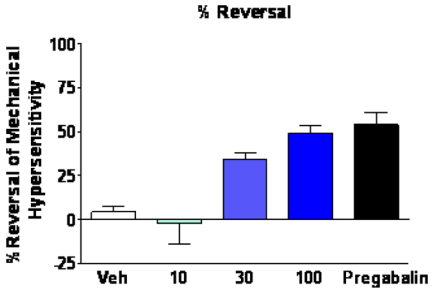

Figure 10. Spinal nerve ligation assay (neuropathic pain) after oral dosing of compound **11**.

the 2 h time point compared to those measured at 2 h in the CFA study. Again, efficacy was observed at plasma concentration in moderate excess of the cellular IC_{50} when corrected for plasma protein binding (Table 3).

Table 3. Plasma Concentrations in SNL Study

dose (mg/kg)	[plasma] (μM)	$C_{u,plasma}$ (nM)	fold IC_{50}
10	1	5	1×
30	6.7	34	6×
100	23	115	23×

SUMMARY

The intention of this manuscript is to serve as an overview of our efforts to identify novel chemotypes for the development of selective kinase inhibitors. We have identified several series of small molecule inhibitors of TrkA with unique binding modes in the field of kinase inhibitors. The crystallographic structures have been solved for all four inhibitor series with the TrkA kinase domain, and their unique binding modes have been elucidated. These leads were optimized for potency and selectivity. We employed a rational structure based drug design approach to progress these series. During the optimization process we strived to abide by the principles of ligand efficiency

dx.doi.org/10.1021/jm5006429 | J. Med. Chem. XXXX, XXX, XXX–XXX

to maximize binding affinity without relying excessively on lipophilic interactions. While all of the described inhibitor series were found to display very high selectivity against a diverse panel of kinases, because of the high homology in the Trk active site, they exhibited no selectivity versus the other Trk homologues, i.e., TrkB and TrkC, and as such are considered pan-Trk inhibitors. We have also demonstrated efficacy in both inflammatory and neuropathic pain models upon oral dosing. More detailed discussions with respect to the SAR of the individual series and optimization of their physical properties will be the subject of future communications.

EXPERIMENTAL SECTION

General Chemistry Information. Reagents and solvents, including anhydrous THF, dichloromethane, and DMF, were purchased from Aldrich, Acros, or other commercial sources and were used without further purification. Reactions that were moisture sensitive or that required the use of anhydrous solvents were performed under either nitrogen or argon atmosphere. Analytical thin layer chromatography (TLC) was performed on precoated silica gel plates obtained from Analtech. Visualization was accomplished with UV light or by staining with basic $KMnO_4$ solution or ethanolic H_2SO_4 solution. Compounds were purified by flash chromatography using an automated purification system (ISCO, Biotage, Analogix) using disposable silica gel prepacked cartridges. Alternatively, compounds were purified by preparative reverse-phase HPLC using a Gilson 215 liquid handler and a Phenomenex Luna C18 column (150 mm × 20 mm i.d.) with a linear gradient over 15 min (95:5 to 0:100 H_2O containing 0.1% trifluoroacetic acid/acetonitrile or 0.1% formic acid/acetonitrile). NMR spectra were recorded on 400 or 500 MHz on a Bruker or Varian spectrometer with $CDCl_3$ or DMSO-d_6 as solvent. The chemical shifts are given in ppm, referenced to the deuterated solvent signal. Purity of target compounds was determined using LCMS and HPLC. LCMS analyses were performed using an Applied Biosystems API-150 mass spectrometer and Shimadzu SCL-10A LC system: column, Phenomenex Gemini C18, 5 μm, 50 mm × 4.6 mm i.d.; gradient, from 90% water, 10% CH_3CN, 0.05% TFA, 5 min, to 5% water, 95% CH_3CN, 0.05% TFA in 5 min; UV detection, 254 nm. Compound purity was determined by integrating peak areas of the liquid chromatogram, monitored at 254 nm. Purity of targets compounds was ≥95%.

***N*4-(4-Morpholinophenyl)-*N*6-(pyridin-3-ylmethyl)pyrido-[3,2-*d*]pyrimidine-4,6-diamine (1).** *Step 1.* Commercially available 4,6-dichloropyrido[3,2-*d*]pyrimidine (0.20 g, 1.0 mmol), 4-morpholinoaniline (0.19 g, 1.1 mmol), and DIPEA (0.18 mL, 1.1 mmol) were dissolved in DMF (3 mL), and the mixture was stirred at 80 °C for 12 h. The reaction mixture was cooled to room temperature, and water (30 mL) was added. The aqueous solution was extracted using ethyl acetate (3 × 50 mL). The combined organic layers were dried over $MgSO_4$, filtered, and concentrated. The crude product was purified using silica gel chromatography (24 Gm Si gel, 0–20% MeOH in DCM) to afford 6-chloro-*N*-(4-morpholinophenyl)pyrido[3,2-*d*]-pyrimidin-4-amine (0.34 g, 99% yield). ^{1}H NMR (400 Hz, $CDCl_3$) δ 8.76 (s, 1H), 8.72 (s, 1 H), 8.10 (d, J = 8.8 Hz, 1 H), 7.76 (d, J = 8.8 Hz, 2 H), 7.67 (d, J = 8.8 Hz, 1H), 6.99 (d, J = 9.0 Hz, 2 H), 3.88 (m, 4H), 3.18 (m, 4 H). LRMS, M + H: 342.8.

Step 2. A solution of 6-chloro-*N*-(4-morpholinophenyl)pyrido[3,2-*d*]pyrimidin-4-amine (0.15 g, 0.44 mmol), pyridin-3-ylmethane amine (0.10 g, 0.88 mmol), and DIPEA (0.15 mL, 0.88 mmol) in NMP (3 mL) was heated to 90 °C for 48 h. The reaction mixture was then cooled, diluted with water (30 mL), and extracted with EtOAc (3 × 50 mL). The combined organic layers were dried over $MgSO_4$, filtered, and concentrated. The crude product was purified using silica gel chromatography (24 Gm Si gel, 0–20% MeOH in DCM) to afford *N*4-(4-morpholinophenyl)-*N*6-(pyridin-3-ylmethyl)pyrido[3,2-*d*]-pyrimidine-4,6-diamine (0.09 g, 51%). ^{1}H NMR (400 Hz, $CDCl_3$) δ 8.74 (s, 1H), 8.57 (d, J = 4.9 Hz, 1 H), 8.54 (s, 1H), 8.44 (s, 1H), 7.87 (d, J = 8.8 Hz, 1H), 7.75 (d, J = 7.8 Hz, 1H), 7.70 (d, J = 9.0 Hz, 2H), 7.30 (m, 1H), 6.98–6.94 (m, 3H), 5.33 (m, 1H), 4.75 (d, J = 5.6 Hz, 2H), 3.88 (m, 4H), 3.15 (m, 4H). HRMS (ESI): m/z calculated for $C_{23}H_{23}N_7O$ = 413.1964. Found $[M + H]^+$: 414.2048.

***N*-(3-Cyclopropyl-1-phenyl-1*H*-pyrazol-5-yl)-2-(4-(3-methoxy-4-(4-methyl-1*H*-imidazol-1-yl)phenyl-1*H*-1,2,3-triazol-1-yl)acetamide (2).** *Step 1.* To a stirred solution of 3-cyclopropyl-1-phenyl-1*H*-pyrazol-5-amine (2.00 g, 10.0 mmol) and Et_3N (1.32 g, 13.1 mmol) in THF (50 mL) at room temperature was added 2-chloroacetyl chloride (1.36 g, 12.1 mmol) dropwise. After being stirred overnight, the reaction mixture was concentrated. The crude product was purified by silica gel chromatography (80 g SiO_2, 3–50% EtOAc in hexanes) to afford 2-chloro-*N*-(3-cyclopropyl-1-phenyl-1*H*-pyrazol-5-yl)acetamide (2.3 g, 82%). LRMS: $[M + H]^+$ 276.0.

Step 2. A mixture of 2-chloro-*N*-(3-cyclopropyl-1-phenyl-1*H*-pyrazol-5-yl)acetamide (2.77 g, 10.1 mmol) and NaN_3 (0.98 g, 15.1 mmol) in EtOH (35 mL) was heated at 60 °C for 16 h. The reaction mixture was concentrated, diluted with water, and extracted with EtOAc (3 × 30 mL). The combined organic extracts were dried over Na_2SO_4 and concentrated. Purification by silica gel chromatography (80 g SiO_2, 3–60% EtOAc in hexanes) afforded 2-azido-*N*-(3-cyclopropyl-1-phenyl-1*H*-pyrazol-5-yl)acetamide (2.0 g, 71%). LRMS: $[M + H]^+$ 283.1.

Step 3. To a solution of 2-azido-*N*-(3-cyclopropyl-1-phenyl-1*H*-pyrazol-5-yl)acetamide (0.596 g, 2.11 mmol) and 1-(4-ethynyl-2-methoxyphenyl-4-methyl-1*H*-imidazole (0.471 g, 2.22 mmol) in 1:1 *tert*-butanol/water (12 mL) was added a 1 M solution of copper(II) sulfate (0.422 mL, 0.422 mmol) and copper dust (0.107 g, 1.69 mmol), and the mixture was heated in a sealed vial at 125 °C for 1 h. The mixture was cooled and diluted with water. Concentrated ammonium hydroxide was added to convert all of the remaining copper to copper–hexaamine complex and extracted with EtOAc (3 × 15 mL). The combined organics were dried over sodium sulfate, filtered, and concentrated. Purification by silica gel chromatography (isocratic 10% MeOH/EtOAc) afforded *N*-(3-cyclopropyl-1-phenyl-1*H*-pyrazol-5-yl)-2-(4-(3-methoxy-4-(4-methyl-1*H*-imidazol-1-yl)-phenyl-1*H*-1,2,3-triazol-1-yl)acetamide (0.6 g, 58%). ^{1}H NMR (400 MHz, DMSO-d_6) δ 10.59 (s, 1 H), 9.38 (s, 1H), 8.76 (s, 1H), 7.79 (m, 2H), 7.67 (m, 2H), 7.52 (m, 3H), 7.40 (m, 1H), 6.20 (s, 1H), 5.42 (s, 2H), 3.96 (s, 3H), 2.36 (s, 3H), 1.94 (m, 1H), 0.91 (m, 2H), 0.69 (m, 2H). HRMS calculated for $C_{27}H_{26}N_8O_2$, 494.2179; found (ES) m/z $[M + H]^+$, 495.2251.

1-Cyclopropyl-1-(3-(thiazol-2-yl)benzyl)-3-(4-(trifluoromethoxy)phenyl)urea (3). *Step 1.* A 20 L flask fitted with an overhead mechanical stirrer was charged with 4.1 L of toluene, followed by aqueous K_2CO_3 (4.5 L, 1M). The reaction mixture was stirred and degassed with nitrogen over 15–30 min, after which 2-bromothiazole (325 g, 1.8 mol) was quickly charged to the flask. The solution was degassed with stirring for a further 30 min. Tetrakis-(triphenylphosphine)palladium(0) (41.6 g, 0.036 mol) was added to the mixture under an inert atmosphere and the mixture degassed over 30 min. 3-(Formylphenyl)boronic acid (270 g, 1.98 mol) was dissolved in ethanol (2 L) in a 5 L conical flask and the suspension degassed with nitrogen (30 min). The ethanol mixture was rapidly charged to the 20 L flask and the reaction mixture degassed for a further 30 min. With vigorous stirring the mixture was heated at 80 °C under an atmosphere of nitrogen overnight (12 h). Approximately 2–4 L of solvent was initially distilled from the reaction to aid the workup procedure. Upon cooling, the reaction solution was transferred to a sinter using a siphon and filtered through Celite. The Celite was washed with toluene (2 × 500 mL) and the combined organic layer separated. The aqueous layer was then washed with successive portions of toluene (2 × 2 L), and the organic layers were combined and washed with 1 M aqueous K_2CO_3 (2 × 2.5 L). The organic phase was separated, dried over $MgSO_4$ and filtered through Celite. The solvent was removed in vacuo to provide 3-(thiazol-2-yl)benzaldehyde (356.9 g, 59%).

Step 2. 3-(Thiazol-2-yl)benzaldehyde (13.1 g, 0.069 mol) was charged to a 250 mL flask, followed by 65 mL of THF and TMOF (7.51 mL, 0.069 mol). Cyclopropylamine (5.90 g, 0.102 mol) was subsequently added to the flask and the reaction solution shaken

dx.doi.org/10.1021/jm5006429 | J. Med. Chem. XXXX, XXX, XXX–XXX

overnight at room temperature. The solvent was removed in vacuo, and the imine was used directly in the reduction step without further purification. The imine (69 mmol) was dissolved in MeOH (100 mL) and charged to a 250 mL flask. The solution was cooled in an ice bath and $NaBH_4$ (5.20 g, 0.138 mol) was carefully added, maintaining the reaction temperature below 30 °C. The mixture was shaken overnight at room temperature. Reduction of the imine was monitored by HPLC−MS, and upon reaction completion the solution was concentrated to dryness in vacuo, redissolved in ethyl acetate (100 mL), and washed with 1 M aqueous K_2CO_3 (2 × 100 mL). Following separation, the aqueous layer was washed with two further portions of ethyl acetate (2 × 50 mL) and the organic phases were combined, dried over $MgSO_4$, and concentrated in vacuo. PS-CHO (43g, 1.3 mmol/g, 0.6 equiv) and PS-AMPS (29.3 g, 1.9 mmol/g, 0.6 equiv) were transferred to the vessel, and the mixture was shaken at room temperature for 1−2 days. The mixture was filtered. The resin was washed with acetonitrile (2 × 50 mL) and the filtrate concentrated under vacuum. The crude amine was purified by silica gel chromatography (heptane/ethyl acetate; DCM/ethyl acetate) to afford *N*-(3-(thiazo-2-yl)benzyl)cyclopropanamine (9.30 g, 61%).

Step 3. The secondary amine was prepared as a stock solution in DCE to give 0.4 mmol (∼100 mg) per 0.5 mL of solvent and dispensed into a 10 mL plate. A stock solution of 1-isocyanato-4-(trifluoromethoxy)benzene in DCE (0.6 mmol) was added to the amine, and the reaction plate was agitated for 2 days at room temperature. By use of the Radley's Titan resin loader, PS isocyanate (350 mg, 0.4 mmol, 1 equiv, 1.2 mmol/g), and PS-AMPS (210 mg, 0.4 mmol, 1 equiv, 1.9 mmol/g), scavenger resins were added to the reaction plates. A further 2−3 mL of DCE was added to the well to induce resin mobility and the plate was shaken for 2 days at room temperature. The reaction well was individually agitated after 1 day of scavenging. After this scavenging period the DCE solution was removed using a Lissy liquid handler to a 5 mL plate using the following protocol for Lissy transfer from 10 mL plate to 5 mL plate:

(1) Add 1 mL of MeOH to each well, and manually agitate the well.
(2) Transfer 3.5 mL of solvent from the 10 mL master plate to a 5 mL plate using level tracking.
(3) Remove solvent from 5 mL plate in a Genevac.
(4) Add 2 mL of methanol to the well of the 10 mL master plate and mix.
(5) Transfer remaining solvent from the 10 mL master plate to the 5 mL plate using level tracking.
(6) Remove solvent from 5 mL plate in a Genevac.

Purification was performed on a reverse-phase Gilson Prep LC module Xterra Prep MS C18, 50 mm × 19 mm i.d., 5 μm column, with 10 mM ammonium bicarbonate, buffered to pH 10 (water/ACN) over 7 min at [20 mL/min]. Product fractions were concentrated under reduced pressure to afford 1-cyclopropyl-1-(3-(thiazol-2-yl)benzyl)-3-(4-(trifluoromethoxy)phenyl)urea (158 mg, 46%). ^{1}H NMR δ (DMSO-d_6): 8.59 (s, 1H), 7.92 (d, J = 3.2 Hz, 1H), 7.78−7.86 (m, 3H), 7.67−7.69 (m, 2H), 7.48 (t, J = 7.67 Hz, 1H), 7.37 (d, J = 7.6 Hz, 1H), 7.27 (d, J = 8.77 Hz, 2H), 4.62 (s, 2H), 2.62−2.65 (m, 1H), 0.90 (t, J = 6.38 Hz, 2H), 0.77−0.79 (m, 2H). HRMS (ESI), m/z calculated for $C_{21}H_{18}F_3N_3O_2S$: 433.1100. Found $[M + H]^+$: 434.1151.

4-(Naphthylen-10-yl)-1-((5-phenyl-1,2,4-oxadiazol-3-yl)-methyl)-1*H*-pyrrolo[3,2-*c*]pyridine-2-carboxylic Acid (4). Compound **4**, 4-(naphthylen-10-yl)-1-((5-phenyl-1,2,4-oxadiazol-3-yl)-methyl)-1*H*-pyrrolo[3,2-*c*]pyridine-2-carboxylic acid, was part of the HTS screen collection and was not independently synthesized again after validation, as such full experimental procedures are not available, but the final compound has been characterized. ^{1}H NMR ($CDCl_3$): δ 8.78 (d, J = 6.6 Hz, 1H), 8.15−7.95 (m, 3H), 7.86 (d, J = 8.1 Hz, 1H), 7.82 (d, J = 6.8 Hz, 1H), 7.73 (d, J = 7.1 Hz, 1H), 7.59−7.51 (m, 3H), 7.48−7.44 (m, 3H), 7.36 (t, J = 7.6 Hz, 1H), 7.13 (s, 1H), 6.06 (s, 2H). HRMS (ESI): m/z calculated for $C_{27}H_{18}N_4O_3$ 446.1379. Found: $[M + H^+]^+$: 447.1474.

***N*6-(3-Chlorobenzyl)-*N*4-(4-(4-methylpiperazin-1-yl)phenyl)-pyrido[3,2-*d*]pyrimidine-4,6-diamine (5).** *Step 1.* Commercially available 4,6-dichloropyrido[3,2-*d*]pyrimidine (0.20 g, 1.0 mmol), 4-(4-methylpiperazin-1-yl)aniline (0.201 g, 1.05 mmol), and DIPEA (0.183 mL, 1.05 mmol) were dissolved in DMF (3 mL), and the mixture was stirred at 80 °C for 12 h. The reaction mixture was then cooled to room temperature, and water (30 mL) was added. The aqueous solution was extracted with EtOAc (3 × 50 mL). The combined organic layers were dried over $MgSO_4$, filtered, and concentrated. The crude product was purified using silica gel chromatography (24 Gm Si gel, 0−20% MeOH in DCM) to afford 6-chloro-*N*-(4-(4-methylpiperazin-1-yl)phenyl)pyrido[3,2-*d*]-pyrimidin-4-amine (0.21 g, 59% yield). ^{1}H NMR (400 Hz, $CDCl_3$) δ 8.73 (s, 1 H), 8.72 (s, 1H), 8.09 (d, J = 8.8 Hz, 1H), 7.74 (d, J = 8.8 Hz, 2H), 7.66 (d, J = 8.8 Hz, 1H), 7.00 (d, J = 8.8 Hz, 2H), 3.25 (m, 4H), 2.62 (m, 4H), 2.39 (s, 3H). LRMS, M + H: 355.1.

Step 2. A solution of 6-chloro-*N*-(4-(4-methylpiperazin-1-yl)-phenyl)pyrido[3,2-*d*]pyrimidin-4-amine (0.10 g, 0.28 mmol), (3-chlorophenyl)methanamine (0.08 g, 0.56 mmol), and DIPEA (0.098 mL, 0.56 mmol) was dissolved in NMP (3 mL) and heated to 90 °C for 48 h. The reaction mixture was cooled, diluted with water (30 mL), and extracted with EtOAc (3 × 50 mL). The combined organic layers were dried over $MgSO_4$, filtered, and concentrated. The crude product was purified using silica gel chromatography (24 Gm Si gel, 0−20% MeOH in DCM) to afford *N*6-(3-chlorobenzyl)-*N*4-(4-(4-methyl-piperazin-1-yl)phenyl)pyrido[3,2-*d*]pyrimidine-4,6-diamine (0.038 g, 29%). ^{1}H NMR (400 Hz, $CDCl_3$) δ 8.53 (s, 1H), 8.44 (s, 1H), 7.84 (d, J = 9.0 Hz, 1H), 7.67 (d, J = 8.8 Hz, 2H), 7.43 (s, 1 H), 7.31−7.26 (m, 3H), 6.98 (d, J = 8.8 Hz, 2H), 6.93 (d, J = 9.0 Hz, 1H), 5.30 (s, 1H), 4.68 (d, J = 5.4 Hz, 2H), 3.21 (m, 4H), 2.61 (m, 4H), 2.37 (s, 3H). LRMS, M + H: 460.2. HRMS (ESI): m/z calculated for $C_{25}H_{26}ClN_7$ 459.1928. Found $[M + H]^+$: 460.2037.

***N*-(1*H*-Benzimidazol-2-ylmethyl)-6-[(2*R*)-2-(2,5-difluorophenyl)pyrrolidin-1-yl]pyrido[3,2-*d*]pyrimidin-4-amine (6).** *Step 3.* 4-Chloro-6-[(2*R*)-2-(2,5-difluorophenyl)pyrrolidin-1-yl]-pyrido[3,2-*d*]pyrimidine (compound **9**) (10 mg, 0.029 mmol), 1-(1*H*-benzimidazol-2-yl)methanamine (21 mg, 0.087 mmol), and DIPEA (30 μL, 0.17 mmol) were dissolved in 2 mL of EtOH. The vial was irradiated in a microwave reactor at 110 °C for 15 min. The mixture was concentrated and the crude product was purified by reverse phase HPLC (0−95% 0.01% TFA−acetonitrile gradient over 20 min) to afford *N*-(1*H*-benzimidazol-2-ylmethyl)-6-[(2*R*)-2-(2,5-difluorophenyl)pyrrolidin-1-yl]pyrido[3,2-*d*]pyrimidin-4-amine (7.9 mg, 58%) . ^{1}H NMR (400 MHz, $CDCl_3$): δ 10.51 (NH, s, 1 H), 8.65 (s, 1 H), 7.82 (m, 1 H), 7.73 (m, 2 H), 7.46 (dd, J = 6.4, 3.2 Hz, 2 H), 7.07 (m, 1 H), 6.93 (m, 1 H); 6.68 (m, 2 H), 5.52 (d, J = 6.7 Hz, 2 H), 5.17 (m, 1 H), 4.12 (m, 1 H), 3.95 (m, 1 H), 2.68−2.46 (m, 1 H), 2.10 (m, 4 H). HRMS (ES) m/z calculated for $C_{24}H_{21}F_2N_7S$ 477.1547. Found $[M + H^+]^+$: 478.1610.

4-Chloro-6-[(2*R*)-2-(2,5-difluorophenyl)pyrrolidin-1-yl]-pyrido[3,2-*d*]pyrimidine (8). Commerically available 6-chloropyrido[3,2-*d*]pyrimidin-4(3*H*)-one (compound **7**) (250 mg, 1.38 mmol) and (2*R*)-2-(2,5-difluorophenyl)pyrrolidine (504 mg, 2.75 mmol) were dissolved in EtOH (2 mL). The vial was irradiated in a microwave reactor at 150 °C for 2 h. The mixture was concentrated and the crude product was purified by reverse phase HPLC (0−95% 0.01% TFA−acetonitrile gradient over 20 min) to give 4-chloro-6-[(2*R*)-2-(2,5-difluorophenyl)pyrrolidin-1-yl]pyrido[3,2-*d*]pyrimidine (317 mg, 69%). LRMS (ES) m/z M + H calcd, 329; found, 329.

4-Chloro-6-[(2*R*)-2-(2,5-difluorophenyl)pyrrolidin-1-yl]-pyrido[3,2-*d*]pyrimidine (9). 6-[(2*R*)-2-(2,5-Difluorophenyl)-pyrrolidin-1-yl]pyrido[3,2-*d*]pyrimidin-4(3*H*)-one (compound **8**) (465 mg, 1.42 mmol) was suspended in $POCl_3$ (132 μL, 1.42 mmol). The mixture was heated at 100 °C for 2 h. The reaction mixture was added to a mixture of ice, ethyl acetate (20 mL), and aqueous sodium hydrogen carbonate (saturated, 20 mL). The mixture was shaken well, and the aqueous solution was adjusted to be around pH 8. The aqueous layer was extracted with EtOAc (2 × 20 mL). The combined organic fractions were washed with aqueous sodium hydrogen carbonate (saturated, 20 mL), followed by brine and then dried, filtered and the solvent was evaporated under reduced pressure to provide 4-chloro-6-[(2*R*)-2-(2,5-difluorophenyl)pyrrolidin-1-yl]-pyrido[3,2-*d*]pyrimidine (343 mg, 70%). ^{1}H NMR (400 MHz,

dx.doi.org/10.1021/jm5006429 | J. Med. Chem. XXXX, XXX, XXX−XXX

$CDCl_3$): δ 2.05−2.20 (m, 3 H), 2.48−2.61 (m, 1 H), 3.75−4.25 (m, 2 H), 5.20−5.75 (bs, 1 H), 6.74−6.80 (m, 1 H), 6.86−6.96 (m, 1 H), 7.10−7.50 (m, 1 H), 7.92−8.02 (m, 1 H), 8.76 (s, 1 H). LRMS (ES) *m/z* M + H calcd, 347; found, 347.

***N*-(3-Cyclopropyl-1-phenyl-1*H*-pyrazol-5-yl)-2-(4-(4-(4-methyl-1*H*-imidazole-1-yl)phenyl-1*H*-1,2,3-triazol-1-yl)-acetamide (10).** *Step 1.* To a solution of 4-fluorobenzaldehyde (5.00 g, 40.3 mmol) and 4-methyl-1*H*-imidazole (6.68 g, 81 mmol) in DMF (20 mL), under nitrogen, was added K_2CO_3 (8.35 g, 60.4 mmol). The reaction mixture was heated at 100 °C for 19 h. The reaction mixture was cooled to room temperature and diluted with EtOAc (200 mL). The organic solution was washed with saturated aqueous $NaHCO_3$ (2 × 50 mL), dried over Na_2SO_4, and concentrated. Purification by flash chromatography (120 g SiO_2, 0−10% MeOH in DCM) afforded 4-(4-methyl-1*H*-imidazole-1-yl)benzaldehyde (822 mg, 11%). LRMS: $[M + H]^+$ 187.1.

Step 2. To a solution of 4-(4-methyl-1*H*-imidazole-1-yl)-benzaldehyde (500 mg, 2.69 mmol) and dimethyl (1-diazo-2-oxopropyl)phosphonate (619 mg, 3.22 mmol) in anhydrous MeOH (10 mL) was added K_2CO_3 (742 mg, 5.4 mmol). The reaction mixture was stirred at room temperature for 24 h, diluted with DCM (60 mL), and washed with water (1 × 50 mL). The aqueous solution was extracted with DCM (1 × 50 mL). Combined organic extracts were dried over Na_2SO_4 and concentrated. Purification by silica gel chromatography (24 g SiO_2, 0−10% MeOH in DCM) afforded 1-(4-ethynylphenyl)-4-methyl-1*H*-imidazole (466 mg, 95%). LRMS: $[M + H]^+$ 183.1.

Step 3. To a solution of 1-(4-ethynylphenyl)-4-methyl-1*H*-imidazole (43 mg, 0.237 mmol) and 2-azido-*N*-(3-cyclopropyl-1-phenyl-1*H*-pyrazol-5-yl)acetamide (67 mg, 0.237 mmol) in *t*-BuOH−H_2O (1:1, 3 mL) were added copper powder (15 mg, 0.237 mmol) and aqueous $CuSO_4$ (1 M, 0.237 mL). The reaction mixture was heated at 125 °C, under microwave irradiation, for 10 min. After cooling to room temperature, concentrated NH_4OH (10 mL) was added. The mixture was stirred for 5 min, and then the aqueous portion was extracted with EtOAc (3 × 20 mL). Combined organic extracts were dried over Na_2SO_4 and concentrated. Purification by reverse-phase HPLC (5−95% MeCN in water, 0.05% TFA modifier used for the mobile phase) afforded *N*-(3-cyclopropyl-1-phenyl-1*H*-pyrazol-5-yl)-2-(4-(4-(4-methyl-1*H*-imidazole-1-yl)phenyl-1*H*-1,2,3-triazol-1-yl)acetamide (37 mg, 34%). ^1H NMR (400 MHz, DMSO-d_6) δ 10.52 (s, 1H), 8.59 (s, 1H), 8.26 (s, 1H), 7.98 (d, *J* = 7.2 Hz, 2H), 7.71 (d, *J* = 7.2 Hz, 2H), 7.53−7.48 (m, 5H), 7.41−7.37 (m, 1H), 6.20 (s, 1H), 5.37 (s, 2H), 2.18 (s, 3H), 1.93−1.87 (m, 1H), 0.92−0.87 (m, 2H), 0.71−0.67 (m, 2H). HRMS calculated for $C_{26}H_{46}N_8O$, 464.2073; found (ES) *m/z* $[M + H]^+$, 465.2145.

2-(4-(6-(1*H*-Imidazol-1-yl)pyridin-3-yl-1*H*-1,2,3-triazol-1-yl)-*N*-(3-*tert*-butyl)-1-(pyridin-3-yl)-1*H*-pyrazol-5-yl)acetamide (11). To a solution of 5-ethynyl-2-(1*H*-imidazol-1-yl)pyridine compound (**14**) (2.30 g, 13.4 mmol) and 2-azido-*N*-(3-cyclopropyl-1-phenyl-1*H*-pyrazol-5-yl)acetamide (compound **15**) (4.07 g, 13.6 mmol) in DCM−*t*-BuOH (1:12, 65 mL) was added copper powder (0.691 g, 10.9 mmol) followed by water (20 mL) and aqueous $CuSO_4$ (1 M, 2.72 mL). The reaction mixture was heated at 90 °C for 2 h, cooled to room temperature, and diluted with EtOAc (300 mL). To the resulting solution were added concentrated NH_4OH (60 mL) and water (20 mL). The biphasic mixture was stirred vigorously for 30 min. Layers were separated. The aqueous solution was saturated with NaCl and extracted with EtOAc (4 × 200 mL). Combined organic extracts were dried over Na_2SO_4 and concentrated. The resulting solid was recrystallized from hot EtOAc to afford 2-(4-(6-(1*H*-imidazol-1-yl)pyridin-3-yl-1*H*-1,2,3-triazol-1-yl)-*N*-(3-*tert*-butyl)-1-(pyridin-3-yl)-1*H*-pyrazol-5-yl)acetamide (4.60 g, 72%). ^1H NMR (400 MHz, DMSO-d_6) δ 10.67 (br, 1H), 8.99 (d, *J* = 0.9 Hz, 1H), 8.81 (d, *J* = 1.4 Hz, 1H), 8.71 (s, 1H), 8.59 (s, 2H), 8.46−8.43 (m, 1H), 8.01−7.93 (m, 3H), 7.56−7.53 (m, 1H), 7.15 (s, 1H), 6.46 (s, 1H), 5.42 (s, 2H), 1.28 (s, 9H). HRMS calculated for $C_{25}H_{24}N_{10}O$, 468.2138; found (ES) *m/z* $[M + H]^+$, 469.2207.

5-Bromo-2-(1*H*-imidazol-1-yl)pyridine (13). *Step 1.* A mixture of commercially available 2,5-dibromopyridine (compound **12**) (2.00 g, 8.44 mmol), imidazole (0.575 g, 8.44 mmol), L-proline (0.194 g, 1.69 mmol), CuI (0.080 g, 0.42 mmol), and K_2CO_3 (2.33 g, 16.89 mmol) in DMSO (8 mL) was heated at 90 °C, under nitrogen, for 15 h. The reaction mixture was then cooled to room temperature and partitioned between ether (200 mL) and water (100 mL). The aqueous layer was separated and extracted with ether (2 × 100 mL). Combined organic extracts were washed with saturated aqueous $NaHCO_3$, dried over Na_2SO_4, and concentrated to afford 5-bromo-2-(1*H*-imidazol-1-yl)pyridine (1.16 g, 61%) which was used as is in the next step. LRMS: $[M + H]^+$ 225.9.

5-Ethynyl-2-(1*H*-imidazol-1-yl)pyridine (14). To a mixture of 5-bromo-2-(1*H*-imidazol-1-yl)pyridine (200 mg, 0.893 mmol), $PdCl_2(PPh_3)_2$ (50 mg, 0.071 mmol), and CuI (27 mg, 0.143 mmol), under nitrogen, were added DMF (4 mL) and Et_3N (1 mL, 7.17 mmol) followed by trimethylsilylacetylene (0.5 mL, 3.57 mmol). The reaction mixture was heated at 90 °C, under nitrogen, for 3 h and then cooled to room temperature, diluted with ether (30 mL), and filtered through a pad of Celite. The filtrate was washed with water (1 × 20 mL) and brine (1 × 20 mL), dried over Na_2SO_4, and concentrated. Purification by silica gel chromatographic (12 g SiO_2, 70−100% EtOAc in hexanes) afforded 2-(1*H*-imidazol-1-yl)-5-((trimethylsilyl)-ethynyl)pyridine (167 mg, 78%). LRMS: $[M + H]^+$ 242.1.

Step 2. Potassium fluoride (48 mg, 0.83 mmol) was added to a solution of 2-(1*H*-imidazol-1-yl)-5-((trimethylsilyl)ethynyl)pyridine (166 mg, 0.688 mmol) in MeOH (1 mL) and stirred at room temperature for 1 h. The reaction mixture was diluted with water and extracted with DCM (3 × 10 mL). Sodium chloride was then added to the aqueous solution until saturation and extracted with EtOAc (2 × 10 mL). The combined organic extracts were dried over Na_2SO_4 and concentrated to provide 5-ethynyl-2-(1*H*-imidazol-1-yl)pyridine (116 mg, 100%). LRMS: $[M + H]^+$ 170.1.

2-Azido-*N*-(3-(*tert*-butyl)-1-(pyridin-3-yl)-1*H*-pyrazol-5-yl)-acetamide (15). To a stirring solution of commercially available 3-(*tert*-butyl)-1-(pyridin-3-yl)-1*H*-pyrazol-5-amine (compound **16**) (700 mg, 3.24 mmol) and Et_3N (426 mg, 4.21 mmol) in DCM (12 mL) at 0 °C was added 2-chloroacetyl chloride (439 mg, 3.88 mmol) dropwise. After 20 min, the reaction mixture was concentrated and purified by silica gel chromatography (40 g SiO_2, 10−100% EtOAc in hexanes) to afford *N*-(3-(*tert*-butyl)-1-(pyridin-3-yl)-1*H*-pyrazol-5-yl)-2-chloroacetamide (682 mg, 72%). LRMS: $[M + H]^+$ 293.0.

A mixture of *N*-(3-(*tert*-butyl)-1-(pyridin-3-yl)-1*H*-pyrazol-5-yl)-2-chloroacetamide (682 mg, 2.33 mmol) and NaN_3 (227 mg, 3.49 mmol) in EtOH (25 mL) was heated at 60 °C for 16 h. The reaction mixture was concentrated, diluted with water, and extracted with EtOAc (3 × 100 mL). Combined organic extracts were dried over Na_2SO_4 and concentrated. Purification by silica gel chromatographic (24 g SiO_2, 30−100% EtOAc in hexanes) afforded 2-azido-*N*-(3-(*tert*-butyl)-1-(pyridin-3-yl)-1*H*-pyrazol-5-yl)acetamide (640 mg, 92%). LRMS: $[M + H]^+$ 300.1.

1-Isopropyl-1-(3-(thiazol-2-yl)benzyl)-3-(4-(trifluoromethoxy)phenyl)urea (17). *Step 1.* To a solution of *N*-(3-(thiazol-2-yl)phenyl)methanamine (1.23 g, 6.46 mmol) in dichloroethane (20 mL) was added acetone (0.32 mL, 4.30 mmol) followed by acetic acid (0.26 mL, 4.30 mmol). The reaction mixture was allowed to stir for 10 min after which a white solid precipitated. To the mixture was then added sodium triacetoxy borohydride (1.37 g, 6.46 mmol), and the mixture was allowed to stir at ambient temperature for 16 h. The reaction mixture was concentrated under reduced pressure and partitioned between 1 N NaOH (50 mL) and ethyl acetate (3 × 50 mL). The combined organic layers were washed with water (1 × 50 mL) followed by brine (1 × 50 mL). The combined organic layers were dried over sodium sulfate, filtered, and concentrated under reduced pressure. Purification by silica gel chromatography (80 g SiO_2, 5−10% MeOH/DCM over 45 min) afforded *N*-(3-(thiazol-2-yl)-benzyl)propan-2-amine (782 mg, 78%). ^1H NMR δ ($CDCl_3$): 7.94 (s, 1 H), 7.81−7.86 (m, 2 H), 7.39−7.40 (m, 2 H), 7.33 (d, *J* = 3.3 Hz, 1 H), 3.85 (s, 2 H), 2.86−2.92 (m, 1 H), 1.12 (d, *J* = 6.2 Hz, 6 H). LCMS: *m/z* $[M + H^+]$ = 233.1.

Step 2. To a solution of *N*-(3-(thiazol-2-yl)benzyl)propan-2-amine (150 mg, 0.65 mmol) in dichloroethane (2 mL) was added 4-

dx.doi.org/10.1021/jm5006429 | J. Med. Chem. XXXX, XXX, XXX−XXX

(trifluoromethoxy)phenyl isocyanate (131 mg, 0.65 mmol). The mixture was stirred at ambient temperature for 2 h, concentrated under reduced pressure. Purification by silica gel chromatography (40 g SiO_2, 0−50% ethyl acetate/hexanes, over 45 min) afforded 1-isopropyl-1-(3-(thiazol-2-yl)benzyl)-3-(4-(trifluoromethoxy)phenyl)-urea (263 mg, 94%). ^{1}H NMR δ ($CDCl_3$): 8.00 (1 H, s), 7.88−7.91 (m, 2 H), 7.37−7.51 (m, 3 H), 7.20 (d, J = 8.7 Hz, 2 H), 7.06 (d, J = 8.6 Hz, 2 H), 6.23 (s, 1 H), 4.70−4.77 (m, 1 H), 4.53 (s, 2 H), 1.26 (d, J = 6.8 Hz, 6 H). HRMS (ESI), m/z calculated for $C_{21}H_{20}F_3N_3O_2S$: 436.1301. Found: $[M + H]^+$ 436.1301.

1-((1*H*-Pyrrolo[2,3-*b*]pyridin-3-yl)methyl)-1-isopropyl-3-(4-(trifluoromethoxy)phenyl)urea (18). *Step 1.* To a solution of isopropylamine (0.360 g, 6.09 mmol) in methanol (10 mL) was added commercially available 1-(*tert*-butoxycarbonyl)-3-formyl-7-azaindole (compound **20**) (1.50 g, 6.09 mmol). The mixture was stirred at ambient temperature for 2 h to allow for imine formation. Sodium borohydride was added (0.576 g, 15.2 mmol) and stirred for 16 h at ambient temperature. The solution was concentrated under reduced pressure and partitioned between ether (50 mL) and 10% potassium carbonate (50 mL). Extraction was with ether (2 × 50 mL). The combined organic layers were washed with water (10 mL) and brine (10 mL), dried over sodium sulfate, filtered, and concentrated under reduced pressure to provide *N*-((1*H*-pyrrolo[2,3-*b*]pyridin-3-yl)-methyl)propan-2-amine (compound **21**) that was used for step 2 without additional purification. LCMS: m/z $[M + H^+]$ = 290.2.

Step 2. To a solution of the crude *N*-((1*H*-pyrrolo[2,3-*b*]pyridin-3-yl)methylpropan-2- amine (100 mg, 0.528 mmol) in dichloromethane (20 mL) was added 1-isocyanato-4-(trifluoromethoxy)benzene (0.08 mL, 0.528 mmol). The mixture was allowed to stir at ambient temperature for 30 min. The mixture was concentrated under reduced pressure, dissolved in 2 mL of DMSO, and injected on a Gilson preparative reversed-phase HPLC instrument (Waters Sun Fire Prep C18 5 μm, 30 mm × 150 mm column, 5−95% CH_3CN/water + 0.1% TFA over 15 min at 40 mL/min with a 2 min start collection time). The desired product fractions were combined, and saturated sodium carbonate was added until pH 12 (5 mL) was obtained. The aqueous portion was extracted with EtOAc (3 × 50 mL). The combined organic layers were washed with water (25 mL) and brine (50 mL), dried over sodium sulfate, filtered, and concentrated to afford 1-((1*H*-pyrrolo[2,3-*b*]pyridin-3-yl)methyl)-1-isopropyl-3-(4-(trifluoromethoxy)phenyl)urea (97 mg, 98%). ^{1}H NMR δ ($CDCl_3$): 9.35 (s, 1 H), 8.38 (d, J = 4.6 Hz, 1 H), 7.99 (d, J = 7.9 Hz, 1 H), 7.32 (s, 1 H), 7.13−7.16 (m, 3 H), 7.03 (d, J = 8.6 Hz, 2 H), 6.52 (s, 1 H), 4.69−4.76 (m, 1 H), 4.59 (s, 2 H), 1.23−1.28 (d, J = 6.9 Hz, 6 H). HRMS (ESI): m/z calculated for $C_{19}H_{19}F_3N_4O_2$: 392.1460. Found: $[M + H]^+$ 393.1533.

1-(3-(Thiazol-2-yl)benzyl)-3-(4-(trifluoromethoxy)phenyl)-urea (19). To a solution of (3-1,3-thiazol-2-yl)phenyl)methylamine (170 mg, 0.893 mmol) in hexane (10 mL) and EtOAc (3 mL) was added 4-(trifluoromethoxy)phenyl isocyanate (200 mg, 0.985 mmol). A white solid precipitated, and the mixture was stirred for 16 h at ambient temperature. The white precipitate was filtered, washed with hexanes, and dried to provide 1-(3-(thiazol-2-yl)benzyl)-3-(4-(trifluoromethoxy)phenyl)urea. ^{1}H NMR δ (DMSO-d_6): 8.86 (s, 1 H), 7.92−7.93 (m, 2 H), 7.77−7.82 (m, 2 H), 7.41−7.53 (m, 4 H), 7.23 (d, J = 8.6 Hz, 2 H), 6.81 (t, J = 6.0 Hz, 1 H), 4.39 (d, J = 5.9 Hz, 2 H). LCMS $[M + H]^+$ = 394.1.

4-(3-Ethoxyphenyl)-1-(2-phenoxyethyl)-1*H*-pyrrolo[3,2-*c*]-pyridine-2-carboxylic Acid (22). *Step 1.* To a solution of (racemic)-benzyloxycarbonyl-α-phosphonoglycine trimethyl ester (12.1 g, 36.5 mmol) in 80 mL of dichloromethane was added DBU (6.34 mL, 42.1 mmol) slowly at room temperature. After 30 min a solution of 2-chloro-3-formyl-4-iodopyridine (7.5 g, 28.0 mmol) in CH_2Cl_2 (20 mL) was added slowly at room temperature. During the addition the reaction became slightly exothermic and the mixture was cooled via a cold water bath. After 4 h the mixture was diluted with dichloromethane and washed with 1 N aqueous HCl (2 × 20 mL) and water (1 × 30 mL). The organic layer was dried over $MgSO_4$, filtered, and concentrated. Purification by silica gel chromatography (ISCO RediSep, 330 g SiO_2, 20% EtOAc/hexanes) afforded methyl (2*Z*)-2-{[(benzyloxy)carbonyl]amino}-3-(2-chloro-4-iodopyridin-3-yl)prop-2-enoate (11.46 g, 86%). ^{1}H NMR (400 MHz, $CDCl_3$): δ 7.89 (d, J = 5.1 Hz, 1 H); 7.70 (d, J = 5.1 Hz, 1 H); 7.33 (m, 3 H); 7.24 (m, 2 H); 7.06 (s, 1 H); 6.96 (s, 1 H); 4.97 (s, 2 H); 3.91 (s, 3 H).

Step 2. Methyl (2*Z*)-2-{[(benzyloxy)carbonyl]amino}-3-(2-chloro-4-iodopyridin-3-yl)prop-2-enoate (11.46 g, 24.25 mmol), K_2C0_3 (10.05 g, 72.7 mmol), CuI (0.462 g, 2.43 mmol), and L-proline (0.558 g, 4.85 mmol) were combined in 1,4-dioxane (120 mL). The mixture was degassed (3 × pump/N_2) and heated to reflux. After being stirred at reflux overnight, the mixture was cooled to room temperature and diluted with saturated aqueous 1 N HCl and extracted with dichloromethane (3 × 50 mL). The combined organic layers were dried over $MgSO_4$, filtered through a pad of Celite, and concentrated. The resulting solid was triturated with Et_2O/hexanes to give methyl-4-chloro-1*H*-pyrrolo[3,2-*c*]pyridine-2-carboxylate (4.6 g, 90%). ^{1}H NMR (400 MHz, $CDCl_3$): δ 9.25 (s, 1 H), 8.18 (d, J = 5.8 Hz, 1 H), 7.35 (d, J = 2.1 Hz, 1 H), 7.29 (d, J = 5.9 Hz, 1 H), 3.99 (s, 3 H).

Step 3. Methyl 4-chloro-1*H*-pyrrolo[3,2-*c*]pyridine-2-carboxylate (1.00 g, 4.75 mmol), 3-ethoxyphenylboronic acid (1.03 g, 6.21 mmol), $Pd(OAc)_2$ (0.064 g, 0.285 mmol), XPhos (0.226 g, 0.475 mmol), and potassium fluoride (0.828 g, 14.2 mmol) were combined in 1,4-dioxane (20 mL). The mixture was degassed (3 × pump/N_2) then heated to 100 °C. After 4 h the mixture was cooled to room temperature, diluted with EtOAc, filtered through a pad of Celite washing with EtOAc, and concentrated. Purification by silica gel chromotography (Biotage-SNAP, 50 g SiO_2, 50% EtOAc/hexanes) provided methyl 4-(3-ethoxyphenyl)-1*H*-pyrrolo[3,2-*c*]pyridine-2-carboxylate (1.02 g, 72.5%). ^{1}H NMR (400 MHz, $CDCl_3$): δ 9.20 (bs, 1 H), 8.51 (d, J = 5.8 Hz, 1 H), 7.54−7.49 (m, 3 H), 7.47−7.38 (m, 1 H), 7.29 (d, J = 5.9 Hz, 1 H), 7.04−7.00 (m, 1 H), 4.14 (q, J = 6.83 Hz, 2 H), 3.97 (s, 3 H), 1.45 (t, J = 7.12 Hz, 3 H).

Step 4. To a solution of methyl 4-(3-ethoxyphenyl)-1*H*-pyrrolo[3,2-*c*]pyridine-2-carboxylate (30 mg, 0.10 mmol) in DMF (0.5 mL) was added NaH (60% dispersion in mineral oil, 5.5 mg, 0.148 mmol) at room temperature. After gas evolution had ceased, 2-bromoethyl phenyl ether (27 mg, 0.13 mmol) was added all at once as a solid. After the mixture was stirred overnight 2 M NaOH (200 mL, 0.40 mmol) was added, and stirring continued at room temperature. After 4 h the mixture was concentrated. The crude material was taken up in DMSO and acidified with TFA. The resulting solution was purified by preparative reversed-phase HPLC (30 mm × 100 mm Phenomenex AXIA-Gemini-NX, 15−40% CH_3CN/water containing 0.1% TFA over 18 min at 50 mL/min) to afford 4-(3-ethoxyphenyl)-1-(2-phenoxyethyl)-1*H*-pyrrolo[3,2-*c*]pyridine-2-carboxylic acid as the TFA salt (39 mg, 75%). ^{1}H NMR (500 MHz, DMSO-d_6): δ 8.59 (d, J = 6.6 Hz, 1 H), 8.17 (s, 1 H), 7.60−7.56 (m, 2 H), 7.52 (m, 1 H), 7.48 (m, 1 H), 7.27−7.19 (m, 3H), 6.92−6.87 (m, 1 H), 6.81 (d, J = 8.1 Hz, 2 H), 5.16 (m, 2 H), 4.37 (m, 2 H), 4.16 (q, J = 6.9 Hz, 2 H), 1.38 (t, J = 6.6 Hz, 3 H). HRMS (ESI) calcd $(M + H)^+$ = 403.1652; found 403.1656.

1-(2-(4-Chlorophenoxy)ethyl)-4-(3-ethoxyphenyl)-1*H*-pyrrolo[3,2-*c*]pyridine-2-carboxylic Acid (23). *Step 1.* To a solution of (±)-benzyloxycarbonyl-α-phosphonoglycine trimethyl ester (12.1 g, 36.5 mmol) in 80 mL of DCM was added DBU (6.34 mL, 42.1 mmol) slowly at room temperature. After 30 min a solution of 2-chloro-3-formyl-4-iodopyridine (7.50 g, 28.0 mmol) in 20 mL of DCM was added slowly at room temperature. During the addition the reaction became slightly exothermic and the mixture was cooled via a cold water bath. After 4 h the mixture was diluted with DCM and washed with 1 N HCl (2 × 50 mL) and H_2O (1 × 50 mL). The organic layer was dried over $MgSO_4$, filtered, and concentrated. Purification by silica gel chromatography (330 g SiO_2, 20% EtOAc/hexanes) afforded (*Z*)-methyl 2-(((benzyloxy)carbonyl)amino)-3-(2-chloro-4-iodopyridin-3-yl)acrylate (11.4 g, 86%). ^{1}H NMR (400 MHz, $CDCl_3$): δ 7.89 (d, J = 5.2 Hz, 1 H), 7.70 (d, J = 5.2 Hz, 1 H), 7.33 (d, J = 6.8 Hz, 3 H), 7.25−7.26 (m, 2 H), 7.06 (s, 1 H), 6.96 (bs, 1 H), 4.97 (s, 2 H), 3.91 (s, 3 H).

Step 2. (*Z*)-Methyl 2-(((benzyloxy)carbonyl)amino)-3-(2-chloro-4-iodopyridin-3-yl)acrylate (11.46 g, 24.25 mmol), K_2CO_3 (10.05 g, 72.7 mmol), copper(I) iodide (0.462 g, 2.425 mmol), and L-proline (0.558

dx.doi.org/10.1021/jm5006429 | J. Med. Chem. XXXX, XXX, XXX−XXX

g, 4.85 mmol) were combined in 1,4-dioxane (120 mL). The mixture was degassed (3 × pump/N_2) and then heated to reflux. After refluxing overnight, the mixture was cooled to room temperature, diluted with saturated aqueous NH_4Cl, and extracted with dichloromethane (3 × 100 mL). The combined organic layers were dried over $MgSO_4$, filtered through a pad of Celite, and concentrated. The resulting solid was triturated with Et_2O/hexanes to provide methyl 4-chloro-1*H*-pyrrolo[3,2-*c*]pyridine-2-carboxylate (4.6 g, 90%). ^{1}H NMR (400 MHz, $CDCl_3$): δ 9.25 (bs, 1 H), 8.18 (d, J = 5.8 Hz, 1 H), 7.35 (d, J = 2.1 Hz, 1 H), 7.29 (d, J = 5.9 Hz, 1 H), 3.99 (s, 3 H).

Step 3. Methyl 4-chloro-1*H*-pyrrolo[3,2-*c*]pyridine-2-carboxylate (1.00 g, 4.75 mmol), 3-ethoxyphenylboronic acid (1.03 g, 6.21 mmol), $Pd(OAc)_2$ (0.064 g, 0.285 mmol), XPhos (0.226 g, 0.475 mmol), and KF (0.828 g, 14.24 mmol) were combined in 1,4-dioxane (20 mL). The mixture was degassed (3 × pump/N_2) and then heated to 100 °C. After 4 h the mixture was cooled to room temperature, diluted with EtOAc, filtered through a pad of Celite washing with EtOAc, and concentrated. Purification by silica gel chromatography (50 g SiO_2, 50% EtOAc/hexanes) afforded methyl 4-(3-ethoxyphenyl)-1*H*-pyrrolo[3,2-*c*]pyridine-2-carboxylate (1.02 g, 72%). ^{1}H NMR (400 MHz, $CDCl_3$): δ 9.20 (s, 1 H), 8.51 (d, J = 5.8 Hz, 1 H), 7.50–7.53 (m, 3 H), 7.43 (t, J = 7.9 Hz, 1 H), 7.29 (d, J = 5.9 Hz, 1 H), 7.02 (dd, J = 8.2, 2.5 Hz, 1 H), 4.14 (q, J = 7.0 Hz, 2 H), 3.97 (s, 3 H), 1.45 (t, J = 7.0 Hz, 3 H).

Step 4. To a solution of methyl 4-(3-ethoxyphenyl)-1*H*-pyrrolo[3,2-*c*]pyridine-2-carboxylate (30 mg, 0.10 mmol) in 0.5 mL of THF was added NaH (60% in mineral oil, 6.0 mg, 0.15 mmol) at room temperature. After gas evolution had ceased 1-(2-bromoethoxy)-4-chlorobenzene (31 mg, 0.13 mmol) was added and the mixture heated to 60 °C. After stirring overnight 0.16 mL of 2 M NaOH was added and heating continued. After 4 h the mixture was cooled to room temperature and concentrated. The crude material was taken up in DMSO (1.0 mL), filtered using a 0.45 μm PTFE syringe filter, then purified by preparative reversed-phase HPLC (CH_3CN/H_2O with 0.1% TFA modifier). Fractions containing pure product were concentrated to afford 1-(2-(4-chlorophenoxy)ethyl)-4-(3-ethoxyphenyl)-1*H*-pyrrolo[3,2-*c*]pyridine-2-carboxylic acid (9.7 mg, 17%) as a TFA salt. ^{1}H NMR (500 MHz, DMSO-d_6): δ 8.51 (d, J = 6.2 Hz, 1 H), 7.88 (bs, 1 H), 7.51 (m, 3 H), 7.46 (s, 1 H), 7.27 (d, J = 8.7 Hz, 2 H), 7.14 (bs, 1 H), 6.84 (d, J = 8.7 Hz, 2 H), 5.07 (m, 2 H), 4.35 (m, 2 H), 4.13 (q, J = 7.0 Hz, 2 H), 1.38 (t, J = 6.9 Hz, 3 H). HRMS $C_{24}H_{21}ClN_2O_4$ $(M + H)^+$ calculated, 437.1263; found, 437.1262.

4-(3-Ethoxyphenyl)1-{2-[4-(trifluoromethoxy)phenoxy]-ethyl}-1*H*-pyrrolo[3,2-*c*]pyridine-2-carboxylic Acid (24). *Step 1.* To a solution of methyl-4-(3-ethoxyphenyl)-1*H*-pyrrolo[3,2-*c*]-pyridine-2-carboxylate (230 mg, 0.776 mmol) in DMF (7 mL) was added NaH (60% dispersion in mineral oil, 40 mg, 1.00 mmol) at room temperature. After gas evolution had ceased 1,2-dibromoethane (1 mL, 11.60 mmol) was added rapidly. After being stirred overnight, the mixture was diluted with water and extracted with EtOAc (3 × 30 mL). The combined organic layers were washed with water and brine and then dried over $MgSO_4$, filtered, and concentrated. Purification by silica gel chromatography (Biotage-SNAP, 25 g SiO_2, 0–50% EtOAc/hexanes) afforded methyl-1-2(bromoethyl)-4-(3-ethoxy-1*H*-pyrrolo-[3,2-*c*]pyridine-2-carboxylate (135 mg, 43%). ^{1}H NMR (400 MHz, $CDCl_3$): δ 8.51 (d, J = 6.0 Hz, 1 H), 7.60 (d, J = 1.0 Hz, 1 H), 7.49–7.45 (m, 2H), 7.40 (m, J = 7.9 Hz, 1 H), 7.31 (dd, J = 6.0, 1.0 Hz, 1 H), 6.99 (ddd, J = 8.2, 2.6, 1.1 Hz, 1 H), 4.92 (t, J = 6.8 Hz, 2 H), 4.12 (q, J = 7.0 Hz, 2 H), 3.91 (s, 3 H), 3.71 (t, J = 7.1 Hz, 2 H), 1.43 (t, J = 7.12 Hz, 2 H).

Step 2. 4-(Trifluoromethoxy)phenol (15.4 mg, 0.086 mmol) and K_2CO_3 (24 mg, 0.17 mmol) were combined in a screw cap vial. To this was added a solution of methyl-1-(2-bromoethyl)-4-(3-ethoxyphenyl)-1*H*-pyrrolo[3,2-*c*]pyridine-2-carboxylate (22 mg, 0.056 mmol) in DMF (0.5 mL). The vial was capped and then heated to 60 °C. After being stirred overnight, the mixture was cooled to room temperature. Then 2 N NaOH (100 mL) was added. After 4 h at room temperature the mixture was concentrated. The crude material was taken up in DMSO and acidified with TFA. The resulting solution was purified by preparative reversed-phase HPLC (21 mm × 100 mm Phenomenex AXIA-Gemini-NX, 20–45% CH_3CN/water containing 0.1% THF over 18 min at 20 mL/min) to afford 4-(3-ethoxyphenyl)1-{2-[4-(trifluoromethoxy)phenoxy]ethyl}-1*H*-pyrrolo[3,2-*c*]pyridine-2-carboxylic acid as the TFA salt (5 mg, 15%). ^{1}H NMR (500 MHz,DMSO-d_6): δ 8.58 (d, J = 6.6 Hz, 1 H), 8.16 (bs, 1 H), 7.58 (m, 2 H), 7.52 (d, J = 7.7 Hz, 1 H), 7.47 (m, 1 H), 7.23 (m, 3H), 6.91 (d, J = 8.8 Hz, 2 H), 5.16 (m, 2 H), 4.40 (m, 2 H), 4.15 (q, J = 6.7 Hz, 2 H), 1.38 (t, J = 7.0 Hz, 3H). HRMS (ESI) calcd (M + H) = 487.1475, found 487.1482.

1-(2-[4-(Trifluoromethoxy)phenoxy)ethyl)-1*H*-pyrrolo[3,2-*c*]-pyridine-2-carboxylic Acid (25). Methyl 4-chloro-1-{2-[4-(trifluoromethoxy)phenoxy]ethyl}-1*H*-pyrrolo[3,2-*c*]pyridine-2-carboxylate (25 mg, 0.060 mmol) was hydrogenated (balloon) with 10% Pd/C (10 mg, 9.40 mmol) in MeOH (3 mL) at room temperature. After 4 h the mixture was filtered using a 0.45 μm PTFE syringe filter and then concentrated. The residue was taken up in 0.5 mL of MeOH. To this was added 2 M NaOH (0.15 mL, 0.300 mmol), and then the mixture was heated to 60 °C. After being stirred overnight the mixture was cooled to room temperature and concentrated. The crude material was taken up in DMSO and acidified with TFA. The resulting solution was filtered using a 0.45 μm PTFE syringe filter and then purified by preparative reversed-phase HPLC (21 mm × 100 mm Phenomenex AXIA-Gemini-NX, 20–45% CH_3CN/water containing 0.1% TFA over 18 min at 20 mL/min) to afford 1-(2-[4-(trifluoromethoxy)phenoxy)-ethyl)-1*H*-pyrrolo[3,2-*c*]pyridine-2-carboxylic acid as the TFA salt (22 mg, 75%). ^{1}H NMR (500 MHz, DMSO-d_6): δ 9.36 (s, 1 H), 8.58 (d, J = 6.7 Hz, 1 H), 8.26 (d, J = 6.8 Hz, 1 H), 7.70 (s, 1 H), 7.22 (d, J = 8.5 Hz, 2H), 6.87 (d, J = 8.6 Hz, 2 H), 5.14 (m, 2 H), 4.38 (m, 2 H). HRMS (ESI) calcd $(M + H)^+$ = 367.0900, found 367.0907.

5-Cyano-1-{2-[4-(trifluoromethoxy)phenoxylethyl}-1*H*-indole-2-carboxylic Acid (26). To a solution ethyl 5-cyano-1*H*-indole-2-carboxylate (37 mg, 0.17 mmol), 2-[4-(trifluoromethoxy)phenoxy]-ethanol (42 mg, 0.19 mmol), and triphenylphosphine (227 mg, 0.518 mmol) in toluene (1 mL) was add DIAD (0.044 mL, 0.225 mmol) dropwise at room temperature, and the mixture was stirred overnight. The mixture was diluted with EtOAc and quenched with water. The two layers were separated, and the aqueous phase was further extracted twice with EtOAc. The combined organic layers were washed with brine, dried over Na_2SO_4, filtered, and concentrated in vacuo. Purification by silica gel chromatography (0–30% EtOAc in hexanes) provided ethyl-5-cyano-l-{2-[4-(trifluoromethoxy)phenoxy]ethyl}-1*H*-indole-2-carboxylate (15 mg, 0.04 mmol) that was subsequently dissolved in THF (1 mL), MeOH (300 μL), and 1 M NaOH (200 μL). The reaction mixture was stirred at room temperature for 5 h, after which water was added, the pH was adjusted to 3 with 1 N HCl, and the solvent was removed in vacuo. EtOAc was added to the resulting aqueous solution. The two layers were separated, and the aqueous phase was further extracted with EtOAc (2 × 10 mL). The combined organic layers were washed with brine, dried over Na_2SO_4, filtered, and concentrated in vacuo to afford 5-cyano-1-{2-[4-(trifluoromethoxy)phenoxylethyl}-1*H*-indole-2-carboxylic acid (13.4 mg, 20%). ^{1}H NMR (400 MHz, $CDCl_3$): δ 8.03 (s, 1H), 7.66 (d, J = 8.8 HZ, 1H), 7.57 (d, J = 8.8 Hz, 1H), 7.39 (s, 1H), 7.07 (d, J = 8.8 Hz, 2H), 6.73 (d, J = 9.2 Hz, 2H), 4.97 (t, J = 5.1 Hz, 2H), 4.46–4.34 (m, 4H), 1.43 (t, J = 7.1 Hz, 3H). HRMS: calcd for $C_{19}H_{13}F_3N_2O_4$ 413.0720. Found: 413.0718.

5-(1*H*-Pyrazol-3-yl)-1-(2-(4-(trifluoromethoxy)phenoxy)-ethyl)-1*H*-indole-2-carboxylic Acid (27). *Step 1.* To a solution of ethyl 5-bromo-1*H*-indole-2-carboxylate (1.7 g, 6.3 mmol), 2-[4-(trifluoromethoxy)phenoxy]ethanol (1.7 g, 7.6 mmol), and triphenylphosphine (3.3 g, 12.7 mmol) in toluene (20 mL) was added DIAD (1.85 mL, 9.5 mmol) dropwise at 0 °C. The mixture was left to warm to room temperature and stirred overnight. The mixture was then concentrated in vacuo and purified by silica gel chromatography (0–20% EtOAc in hexanes) to afford ethyl 5-bromo-1-{2-[4-(trifluoromethoxy)phenoxy]ethyl}-1*H*-indole-2-carboxylate (1.6 g, 52%). ^{1}H NMR (400 MHz, $CDCl_3$): δ 7.79 (s, 1H), 7.45 (s, 1H), 7.25 (m, 2H), 7.01 (d, J = 9.2 Hz, 2H), 6.75 (m, 2H), 4.92 (t, J = 5.6 Hz, 2H), 4.37 (q, J = 6.8 Hz, 2H), 4.32 (t, J = 5.6 Hz, 2H), 1.41 (t, J =

dx.doi.org/10.1021/jm5006429 | J. Med. Chem. XXXX, XXX, XXX–XXX

6.8 Hz, 3H). LRMS (M + H): calcd for $C_{20}H_{18}BrF_3NO_4$ 472.1/474.1. Found: 472.1/474.1.

Step 2. Ethyl 5-bromo-1-{2-[4-(trifluoromethoxy)phenoxy]ethyl}-1*H*-indole-2-carboxylate (812 mg, 1.7 mmol), pinacol borane (873 mg, 3.4 mmol), XPhos (98 mg, 0.21 mmol), and KOAc (540 mg, 5.5 mmol) were combined in dioxane (8 mL). The mixture was degassed under vacuum and back-filled with N_2. Palladium acetate (23 mg, 0.1 mmol) was added, and the mixture was degassed and back-filled again. The mixture was left to stir overnight at 85 °C. EtOAc was added, and the mixture was filtered through a pad of Celite, concentrated in vacuo, and purified by silica chromatography (0−30% EtOAc in hexanes) to provide ethyl 5-(4,4,5,5-tetramethyl-1,3,2-dioxaborolan-2-yl)-1-{2-[4-(trifluoromethoxy)phenoxy]ethyl}-1*H*-indole-2-carboxylate (675 mg, 76%). ^{1}H NMR (400 MHz, $CDCl_3$): δ 8.19 (s, 1H), 7.78 (dd, J = 8.4 Hz, 1.2 Hz, 1H), 7.75 (d, J = 8.8 Hz, 1H), 7.33 (s, 1H), 7.05 (d, J = 8.8 Hz, 2H), 6.77 (m, 2H), 4.95 (t, J = 5.6 Hz, 2H), 4.38 (q, J = 7.2 Hz, 2H), 4.32 (t, J = 5.6 Hz, 2H), 1.42 (t, J = 7.2 Hz, 3H). LRMS (M + H): calcd for $C_{26}H_{30}BF_3NO_6$ 520.3. Found: 520.3.

Step 3. Ethyl 5-(4,4,5,5-tetramethyl-1,3,2-dioxaborolan-2-yl)-1-{2-[4-(trifluoromethoxy)phenoxy]ethyl}-1*H*-indole-2-carboxylate (75 mg, 0.14 mmol), 3-bromo-1-(phenylsulfonyl)-1*H*-pyrazole (83 mg, 0.29 mmol), K_2CO_3 (60 mg, 0.43 mmol), and SPhos (6 mg, 0.014 mmol) were combined in dioxane (2 mL). The reaction was degassed and filled with nitrogen 2×. Water (0.4 mL) was added and purged again with nitrogen. Palladium acetate (1.6 mg, 0.007 mmol) was added under nitrogen, and the mixture was heated to 80 °C overnight. EtOAc was added and the crude mixture was filtered through a pad of Celite, concentrated in vacuo, and purified by silica gel chromatography (0−40% EtOAc in hexanes) to provide ethyl 5-(1-(phenylsulfonyl)-1*H*-pyrazol-3-yl)-1-(2-(4-(trifluoromethoxy)phenoxy)ethyl)-1*H*-indole-2-carboxylate (50 mg, 58%). This material was then dissolved in THF (1 mL) and MeOH (1 mL), and NaOH (1 M, 0.5 mL) was added. The reaction mixture was then heated to 80 °C overnight. The solvent was removed in vacuo and the mixture was dissolved in DMSO, purified by reverse phase HPLC (10−95% ACN in H_2O (with 0.1% TFA)) to afford 5-(1*H*-pyrazol-3-yl)-1-(2-(4-(trifluoromethoxy)phenoxy)ethyl)-1*H*-indole-2-carboxylic acid (22 mg, 28%). ^{1}H NMR (500 MHz, DMSO-d_6): δ 8.07 (s, 1H), 7.77 (d, J = 9.0 Hz, 1H), 7.70 (m, 2H), 7.27 (s, 1H), 7.22 (d, J = 9.0 Hz, 2H), 6.92 (d, J = 9.0 Hz, 2H), 6.69 (d, J = 2 Hz, 1H), 4.98 (t, J = 5.5 Hz, 2H), 4.32 (t, J = 5.5 Hz, 2H). HRMS: calcd for $C_{21}H_{17}F_3N_3O_4$ 432.1166. Found: 432.1183.

■ ASSOCIATED CONTENT

Ⓢ Supporting Information

Experimental procedures for protein crystallography, SPR, and details of in vitro and in vivo assays. This material is available free of charge via the Internet at http://pubs.acs.org.

Accession Codes

Structure coordinates have been deposited in the PDB: codes 4PMT, 4PMP, 4PMS, 4PMM.

■ AUTHOR INFORMATION

Corresponding Author

*Phone: 215-652-2273. Fax: 215-652-7310. E-mail: shawn_stachel@merck.com.

Notes

The authors declare no competing financial interest.

■ ABBREVIATIONS USED

Trk, tropomyosin-related kinase; ATP, adenosine 5′-triphosphate; NGF, nerve growth factor; BDNF, brain-derived neurotrophic factor; NT-3, neurotrophin 3; HTS, high-throughput screening; IGFR1, insulin-like growth factor receptor 1; LE, ligand efficiency; LLE, lipophilic ligand efficiency; SPR, surface plasmon resonance; CFA, complete Freund's adjuvant

■ REFERENCES

(1) Manning, G.; Whyte, D. B.; Martinez, R.; Hunter, T.; Sudarsanam, S. The Protein Kinase Compliment of the Human Genome. *Science* **2002**, *298*, 1912−1934.

(2) Reichardt, L. F. Neurotrophin-Regulated Signalling Pathways. *Philos. Trans. R. Soc. B* **2006**, *361*, 1545−1564.

(3) Watson, J. L.; Allen, S. J.; Dawbarn, D. Targeting Nerve Growth Factor in Pain. *BioDrugs* **2008**, *22*, 349−359.

(4) Wang, T.; Yu, D.; Lamb, M. L. Trk Kinase Inhibitors as New Treatments for Cancer Pain. *Expert. Opin. Ther. Pat.* **2009**, *19*, 305−319.

(5) Lane, N. E.; Schnitzer, T. J.; Birbara, C. A.; Mokhtarani, M.; Shelton, D. L.; Smith, M. D.; Brown, M. T. Tanezumab for the Treatment of Pain from Osteoarthritis of the Knee. *N. Engl. J. Med.* **2010**, *363*, 1521−1531.

(6) Invitrogen 92 member kinase panel used as the general counterscreen at 1 μM to assess kinase selectivity.

(7) Protein crystallography conditions and procedured are described in the Supporting Information.

(8) Structure coordinates have been deposited in the PDB: code 4PMT.

(9) Additional hinge binding TrkA inhibitors have also been previously reported in the literature; see the following: (a) Wang, T.; Lamb, M. L.; Scott, D. A.; Wang, H.; Block, M. H.; Lyne, P. D.; Lee, J. W.; Davies, A. M.; Zhang, H.-J.; Zhu, Y.; Gu, F.; Han, Y.; Wang, B.; Mohr, P. J.; Kaus, R. J.; Josey, J. A.; Hoffmann, E.; Thress, K.; MacIntyre, T.; Wang, H.; Omer, C. A.; Yu, D. Identification of 4-Aminopyrazolylpyrimidines as Potent Inhibitors of Trk Kinases. *J. Med. Chem.* **2008**, *51*, 4672−4684. (b) Hong, S.; Kim, J.; Seo, J. H.; Jung, K. H.; Hong, S.-S.; Hong, S. Design, Synthesis and Evaluation of 3,5-Disubstituted 7-Azaindoles as Trk Inhibitors with Anticancer and Antiangiogenic Activities. *J. Med. Chem.* **2012**, *55*, 5337−5349.

(10) Van Linden, O. P. J.; Kooistra, A. J.; Leurs, R.; de Esch, I. J. P.; de Graff, C. KLIFS: A Knowledge-Based Structural Database To Navigate Kinase−Ligand Interaction Space. *J. Med. Chem.* **2014**, *57*, 249−277.

(11) The cell-based assay is performed using the Discover X-Pathhunter assay platform. Experimental details are described in the Supporting Information.

(12) Bouhana, K. S.; Impastato, R.; Pheneger, J.; Jiang, Y.; Wallace, R. D.; Do, M. G.; Zaute, N. A.; Andrews, S. W. Analgesic Effects of a Potent and Selective Kinase Inhibitor of Neurotrophin Receptors TRKA, TRKB and TRKC. WO2010033941, 2010; WO2010048312, 2010; WO2011006074, 2011; www.arraybiopharma.com.

(13) Green, A.; Li, Y.; Stachel, S. J. Preparation of Pyridotriazole and Benzotriazole Compounds as TrkA Kinase Inhibitors. PCT Int. Appl. WO 2012125667 A1, 2012.

(14) Green, A.; Li, Y.; Stachel, S. J. TrkA kinase Inhibitors Compositions and Methods of Use PCT Int. Appl. WO2012125668 A1, 2012.

(15) Structure coordinates have been deposited with the PDB: code 4PMM.

(16) For an excellent review on type I and type II kinase inhibitors see the following: Zuccotto, F.; Ardini, E.; Casale, E.; Angiolini, M. Through the "Gatekeeper Door": Exploiting the Active Kinase Conformation. *J. Med. Chem.* **2010**, *53*, 2681−2694.

(17) Huse, M.; Kuriyan, J. The Conformational Plasticity of Protein Kinases. *Cell* **2002**, *109*, 275−282.

(18) Albaugh, P.; Fan, Y.; Mi, Y.; Sun, F.; Adrian, F.; Li, N.; Jia, Y.; Sarkisova, Y.; Kreusch, A.; Hood, T.; Lu, M.; Liu, G.; Huang, S.; Liu, Z.; Loren, J.; Tuntland, T.; Karanewsky, D. S.; Seidel, H. M.; Molteni, V. Discovery of GNF-5837, a Selective TRK Inhibitor with Efficacy in Rodent Cancer Tumor Models. *ACS Med. Chem. Lett.* **2012**, *3*, 140−145.

(19) Schindler, T.; Bornmann, W.; Pellicena, P.; Miller, W. T.; Clarkson, B.; Kuriyan, J. Structural Mechanism for STI-571 Inhibition of Abelson Tyrosine Kinase. *Science* **2000**, *289*, 1938−1942.
(20) Stachel, S. J.; Egbertson, M.; Brnardic, E.; Jones, K.; Sanders, J. M.; Henze, D. A. TrkA Kinase Inhibitors, Composition and Methods Thereof. PCT Int. Appl. WO 2013/176970, Nov 2013.
(21) Ghose, A. K.; Herbertz, T.; Pippin, D. A.; Salvino, J. M.; Mallamo, J. P. Knowledge Based Predictions of Ligand Binding Modes and Rational Inhibitor Design for Kinase Drug Discovery. *J. Med. Chem.* **2008**, *51*, 5149−5171.
(22) Dar, A. C.; Lopez, M. S.; Shokat, K. M. Small Molecule Recognition of c-Src via the Imantinib-Binding Conformation. *Chem. Biol.* **2008**, *15*, 1015−1022.
(23) Bhat, R.; Xue, Y.; Berg, S.; Hellberg, S.; Ormo, M.; Nilsson, Y.; Radesater, A.-C.; Jerning, E.; Markgren, P.-O.; Borgegard, T.; Nylof, M.; Gimenez-Cassina, A.; Hernandez, F.; Lucas, J. J.; Diaz-Nido, J.; Avila, J. Structural Insights and Biological Effects of Glycogen Synthase Kinase 3-Specific Inhibitor AR-A014418. *J. Biol. Chem.* **2003**, *278*, 45937−45945.
(24) Boije af Gennas, G.; Mologni, L.; Ahmed, S.; Rajaratnam, M.; Marin, O.; Lindholm, N.; Viltadi, M.; Gambacorti-Passerini, C.; Scappozza, L.; Yli-Kauhaluoma, J. Design, Synthesis, and Biological Activity of Urea Derivatives as Anaplastic Lymphoma Kinase Inhibitors. *ChemMedChem* **2011**, *6*, 1680−1692.
(25) Structure coordinates have been deposited in the PDB: code 4PMP.
(26) (a) Behshad, E.; Klabe, R. M.; Margulis, A.; Becker-Pasha, M.; Rupar, M. J.; Collier, P.; Liu, P. C.; Hollis, G. F.; Burn, T. C.; Wynn, R. Phosphorylation State-Dependent High Throughput Screening of the c-Met Kinase. *Curr. Chem. Genomics* **2010**, *4*, 27−33. (b) Wang, W.; Marimuthi, A.; Tsai, J.; Kumar, A.; Krupka, H. I.; Zhang, C.; Powell, B.; Suzuki, Y.; Nguyen, H.; Tabrizizad, M.; Luu, C.; West, B. L. Structural Characterization of Autoinhibited c-Met Kinase Produced by Coexpression in Bacteria with Phosphatase. *Proc. Natl. Acad. Sci. U.S.A.* **2006**, *103*, 3563−3568.
(27) Whelligan, D. K.; Solanki, S.; Taylor, D.; Thomson, D. W.; Cheung, K.-M. J.; Boxall, K.; Mas-Droux, C.; Barillari, C.; Burns, S.; Grummitt, C. G.; Collins, I.; van Montfort, R. L. M.; Aherne, G. W.; Bayliss, R.; Hoelder, S. Aminopyrazine Inhibitors Binding to Unusual Inactive Conformation of the Mitotic Kinase Nek2: SAR and Structural Characterization. *J. Med. Chem.* **2010**, *53*, 7682−7698.
(28) Structure coordinates have been deposited in the PDB: code 4PMS.
(29) Hanney, B.; Manley, P.; Rudd, M. T.; Sanders J. M.; Stachel, S. J.; Henze, D. TrkA Kinase Inhibitors, Compositions and Methods Thereof. PCT. Int. Appl. WO2013009582 A1, 2013.
(30) Regan, J.; Pargellis, C. A.; Cirillo, P. F.; Gilmore, T.; Hickey, E. R.; Peet, G. W.; Proto, A.; Swinamer, A.; Moss, N. The Kinetics of Binding to p38 MAP Kinase by Analogues of BIRB 796. *Bioorg. Med. Chem. Lett.* **2003**, *13*, 3101−3104.
(31) Pargellis, C.; Tong, L.; Churchill, L.; Cirillo, P. F.; Gilmore, T.; Graham, A. G.; Grob, P. M.; Hickey, E. R.; Moss, N.; Pav, S.; Regan, J. Inhibition of p38 MAP Kinase by Utilizing a Novel Allosteric Binding Site. *Nat. Struct. Biol.* **2002**, *9*, 268−272.
(32) Array BioPharma recently reported on the use of a small molecule pan-Trk inhibitor in models of bone cancer and skeletal fracture pain: (a) Ghilardi, J. R.; Freeman, K. T.; Jimenez-Andrade, J. M.; Mantyh, W. G.; Bloom, A. P.; Kuskowski, M. A.; Mantyh, P. W. Administration of a Tropomysin Receptor Kinase Inhibitor Attenuates Sarcoma-Induced Nerve Sprouting, Neuroma Formation and Bone Cancer Pain. *Mol. Pain* **2010**, *6*, 87−97. (b) Ghilardi, J. R.; Freeman, K. T.; Jimenez-Andrade, J. M.; Mantyh, W. G.; Bloom, A. P.; Bouhana, K. S.; Trollinger, D.; Winkler, J.; Lee, P.; Andrews, S. W.; Kuskowski, M. A.; Mantyh, P. W. Sustained Blockage of Neurotrophin Receptors TrkA, TrkB, and TrkC Reduces Non-Malignant Skeletal Pain but Not the Maintenance of Sensory and Sympathetic Nerve Fibers. *Bone* **2011**, *28*, 389−398.
(33) Wild, K. D.; Bian, D.; Zhu, D.; Davis, J.; Bannon, A. W.; Zhang, T. J.; Louis, J.-C. Antibodies to Nerve Growth Factor Reverse Established Tactile Allodynia in Rodent Models of Neuropathic Pain without Tolerance. *J. Pharmacol. Exp. Ther.* **2007**, *322*, 282−287.